Electronic Supplementary Information (ESI)

Fluorophore unit controlled photoswitching of hydrazone derivatives: Reversible and irreversible off-on/dual-colour fluorescence photoswitches

Deepanjaly K. Sivadas,[a] Sasikala Ravi,[b] Palaniyappan Nagarasu,[a] Delna Johnson,[c] Vijay Thiruvenkatam,[c] Savarimuthu Philip Anthony[b*] and Vedichi Madhu[a*]

[a]*Department of Applied Chemistry, Karunya Institute of Technology and Sciences, Coimbatore-641 114, Tamil Nadu, India. Tel: +91-422-261-4483;*
E-mail: madhu@karunya.edu; vmadhuu1@gmail.com

[b]*School of Chemical & Biotechnology, SASTRA Deemed University, Thanjavur- 613401, Tamil Nadu, India. philip@biotech.sastra.edu*

[c]*Discipline of Biological Engineering, Indian Institute of Technology Gandhinagar, Gandhinagar, Gujarat, 382355, India*

1. Materials and Methods

All solvents and chemicals were purchased from commercial suppliers (Aldrich, Alfa Aesar, Merck and HiMedia) and were used as received. Solvents were purified using appropriate drying agents when necessary. Air and moisture sensitive reactions were carried out under N_2 atmosphere. Fourier transformed infrared (FT-IR) measurements were carried out with Shimadzu IR Affinity-1S spectrophotometer with KBr pellets. ^{1}H and ^{13}C NMR spectra were recorded on Bruker Avance III 400 MHz spectrometer equipped with a 5 mm BBFO probe. The UV−Vis absorption spectra were recorded with UV-Vis-NIR spectrophotometer (Jasco V-770) with $BaSO_4$ as reference, equipped with a diffuse reflectance accessory. Fluorescence spectra and absolute quantum yield for all compounds in the solid state were recorded using Jasco fluorescence spectrometer-FP-8300 instruments equipped with integrating sphere and calibrated light source. Mass spectra were recorded on Micromass ESI-Q-TOF mass spectrometer. Single crystal X-ray diffraction data were collected on a Bruker AXS SMART APEX CCD diffractometer using graphite monochromated MoKa (λ= 0.7107 Å) radiation at 290(2) K and the intensities were measured using ω scan with a scan width of 0.3°. A total of 606 frames per set were collected in different settings of ϕ keeping the sample to detector distance of 6.054 cm. Crystal data were reduced by SAINTPLUS, and an empirical absorption correction was applied using the package SADABS available in the Bruker software package. All the crystal structures were solved by direct methods using SHELXS-97[1] and refined by full-matrix least squares method using SHELXL-97[2] present in the program suite WinGX (Version 1.7.0).

2. Experimental Section

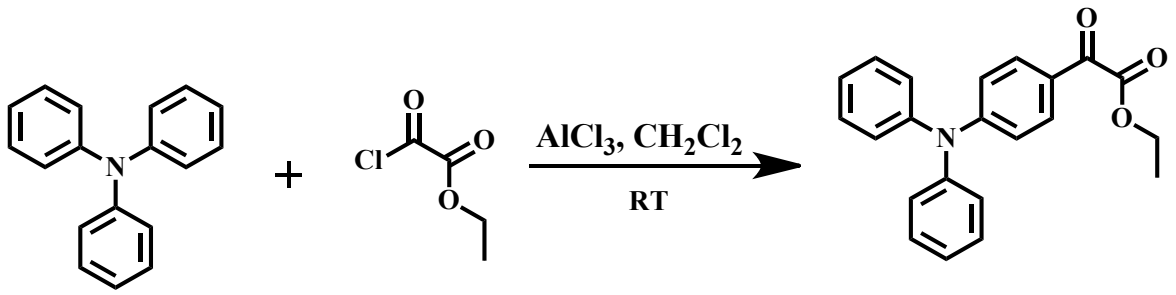

Scheme S1. Synthesis of 1.

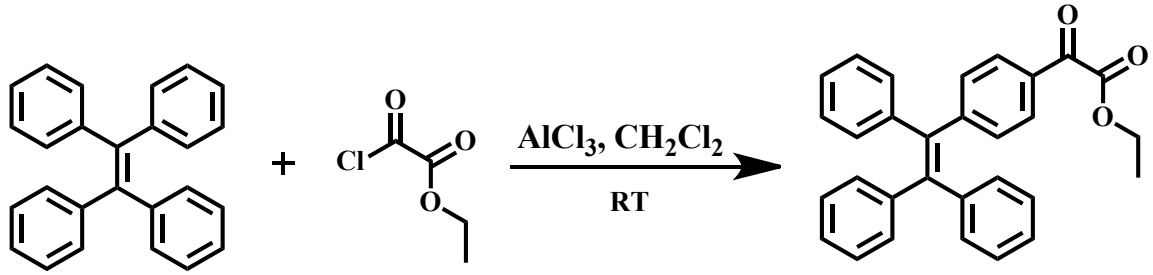

Scheme S2. Synthesis of 2.

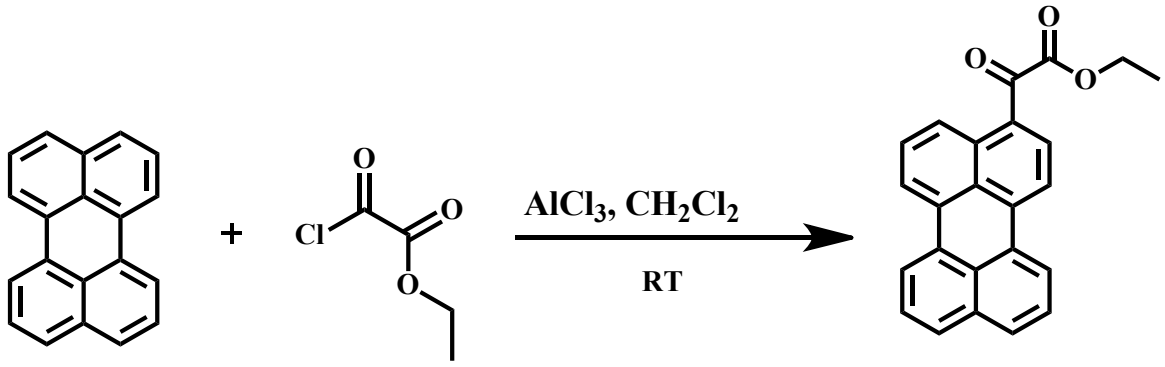

Scheme S3. Synthesis of 3.

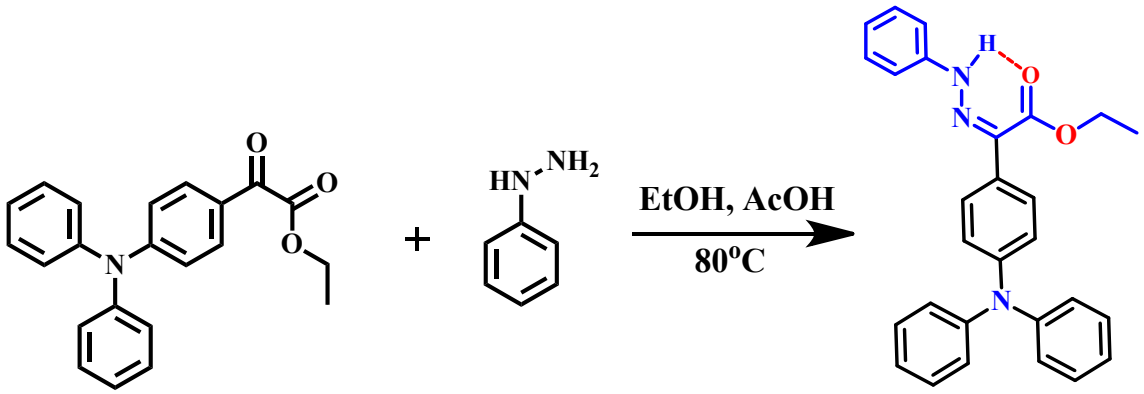

Scheme S4. Synthesis of TPA-PH.

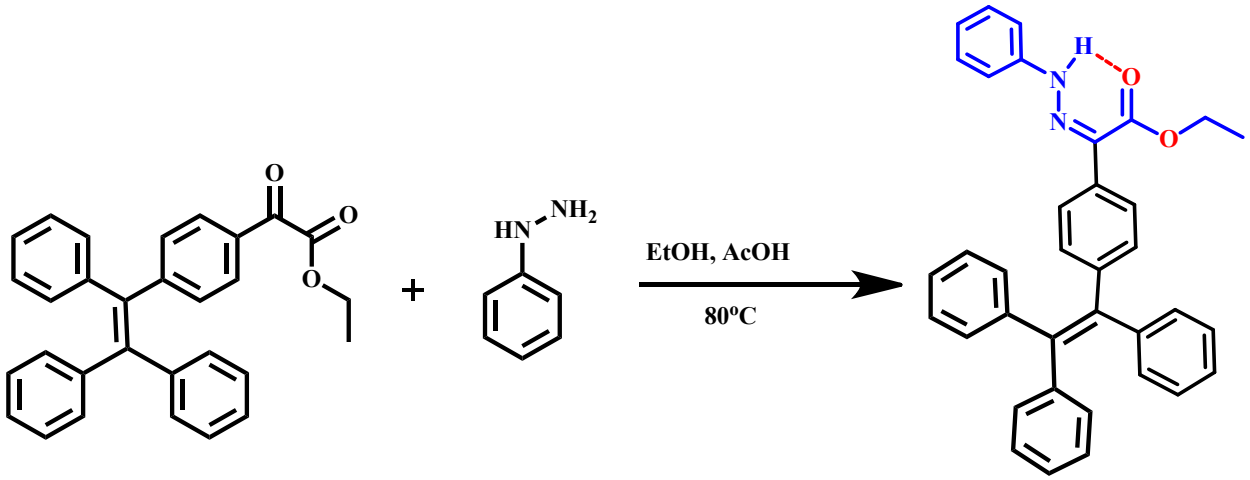

Scheme S5. Synthesis of TPE-PH.

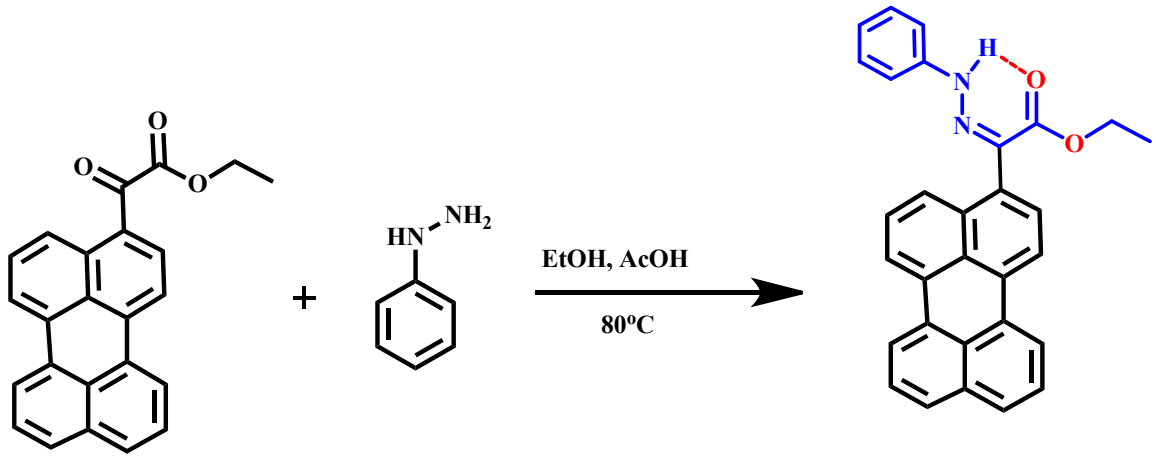

Scheme S6. Synthesis of PY-PH.

3. FT-IR Analysis

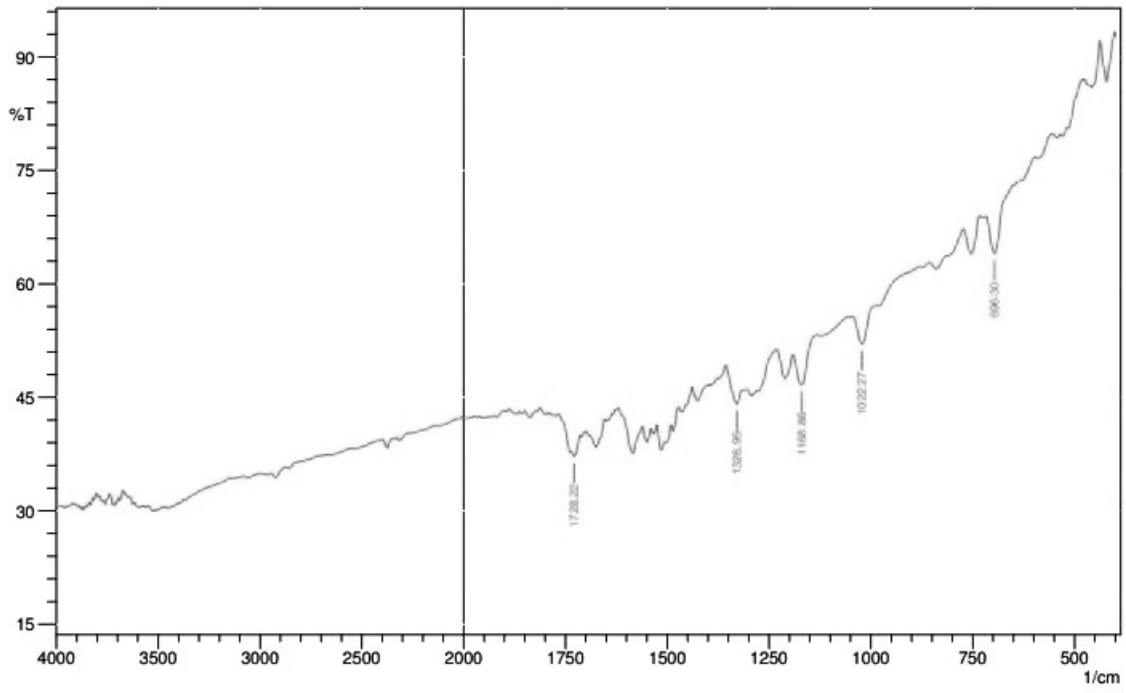

Fig. S1 FT-IR spectrum of 1.

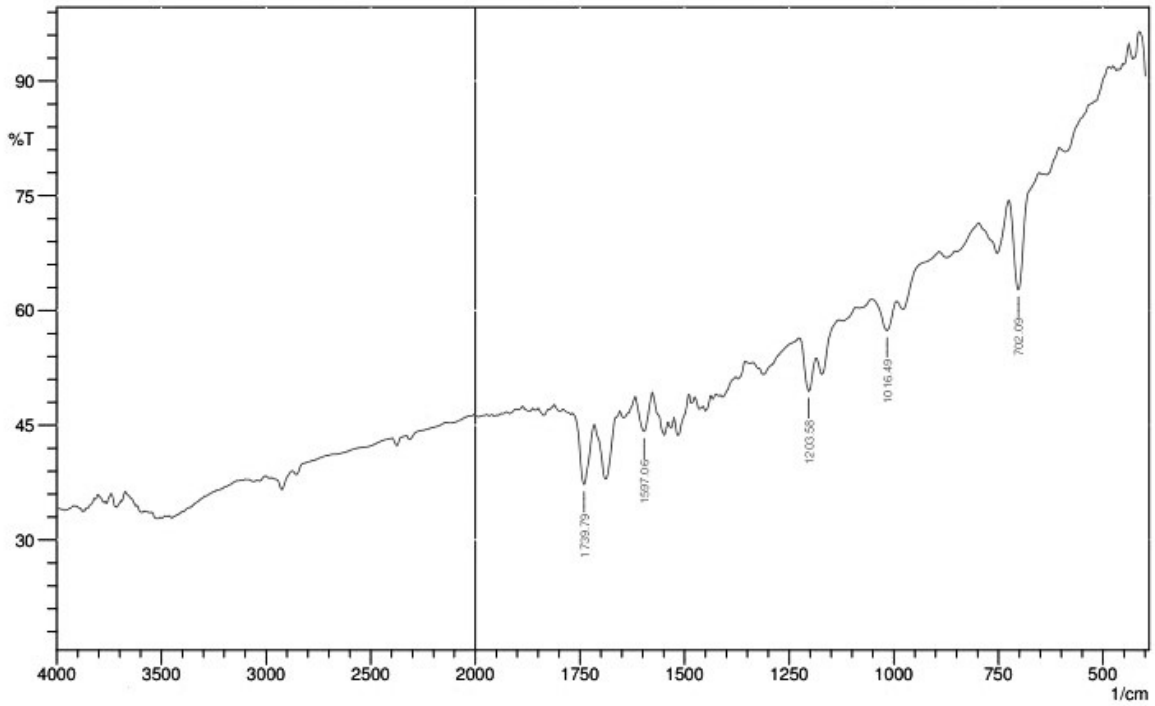

Fig. S2 FT-IR spectrum of 2.

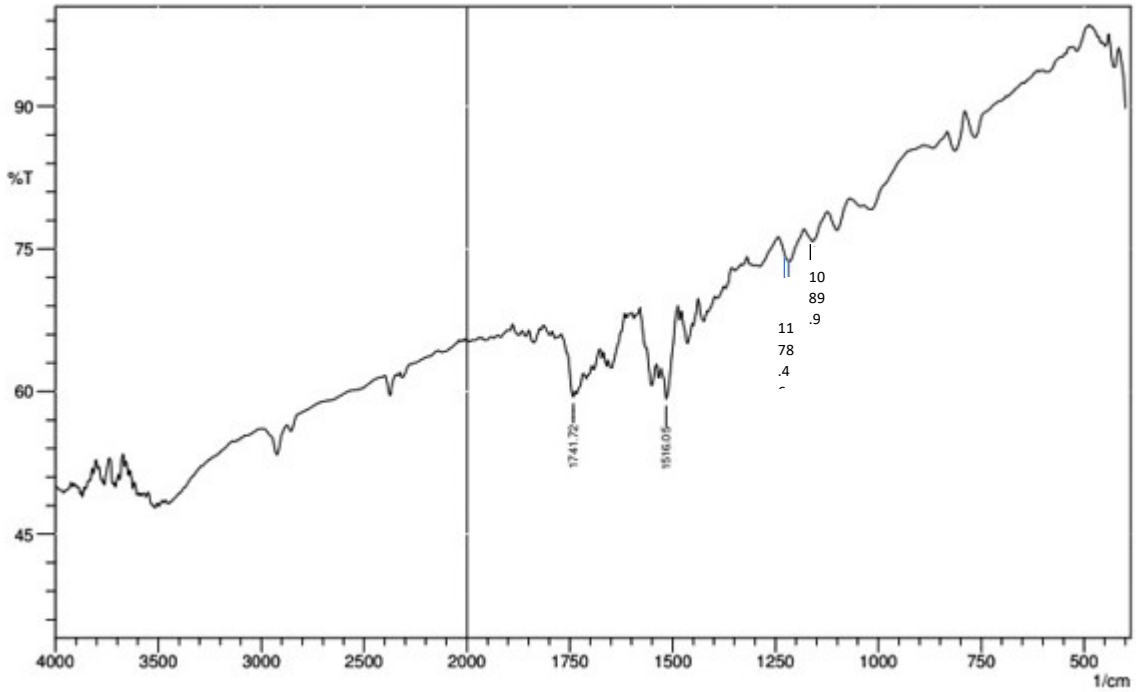

Fig. S3 FT-IR spectrum of 3.

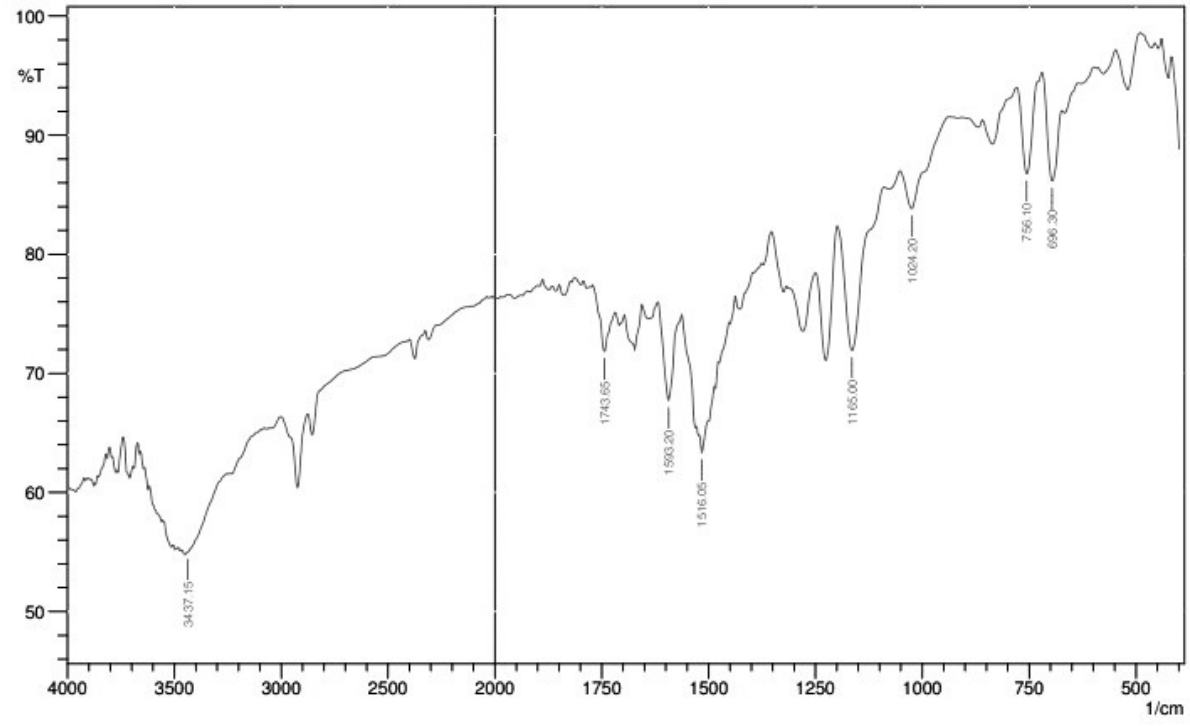

Fig. S4 FT-IR spectrum of TPA-PH.

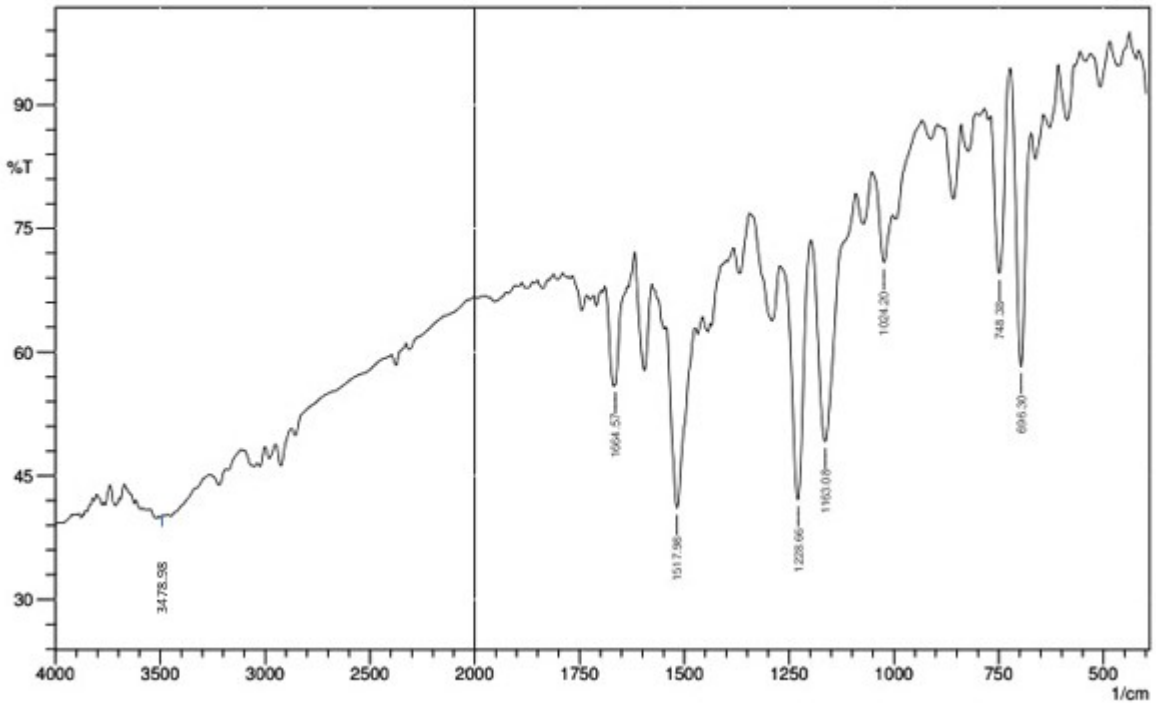

Fig. S5 FT-IR spectrum of TPE-PH.

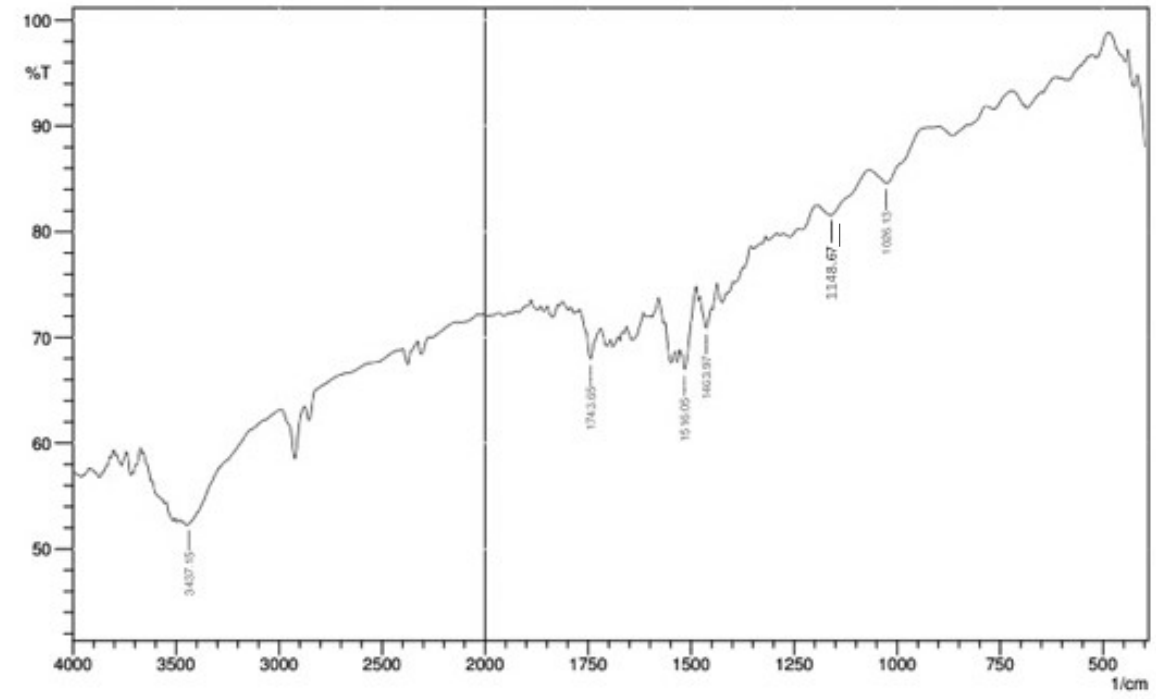

Fig. S6 FT-IR spectrum of PY-PH.

4. NMR Analysis

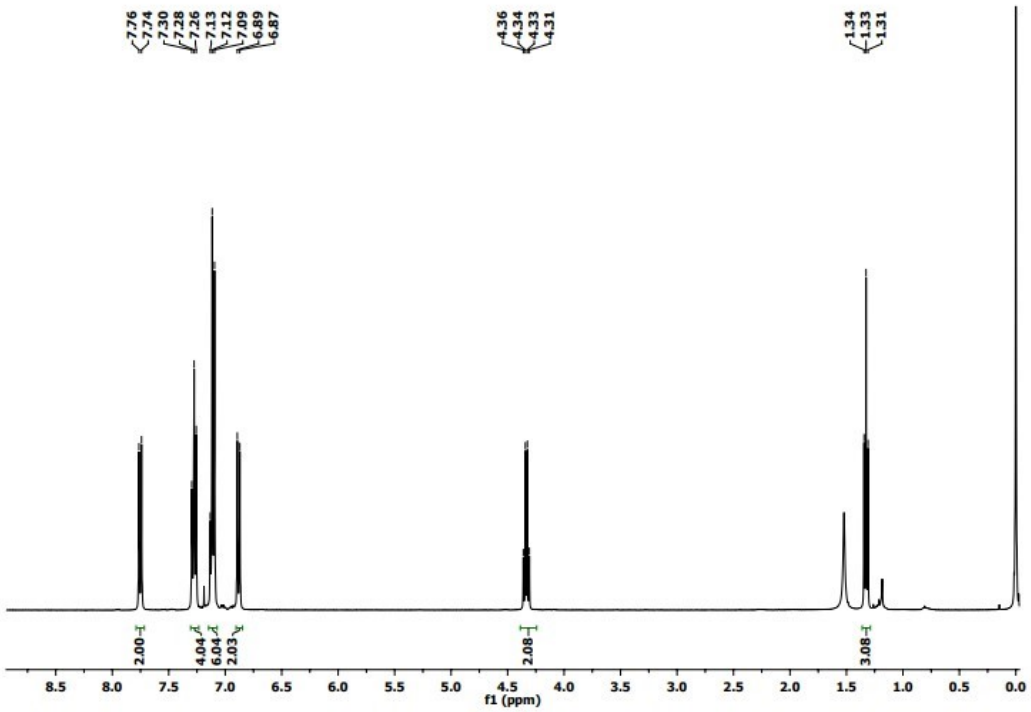

Fig. S7 ^{1}H NMR spectrum of 1.

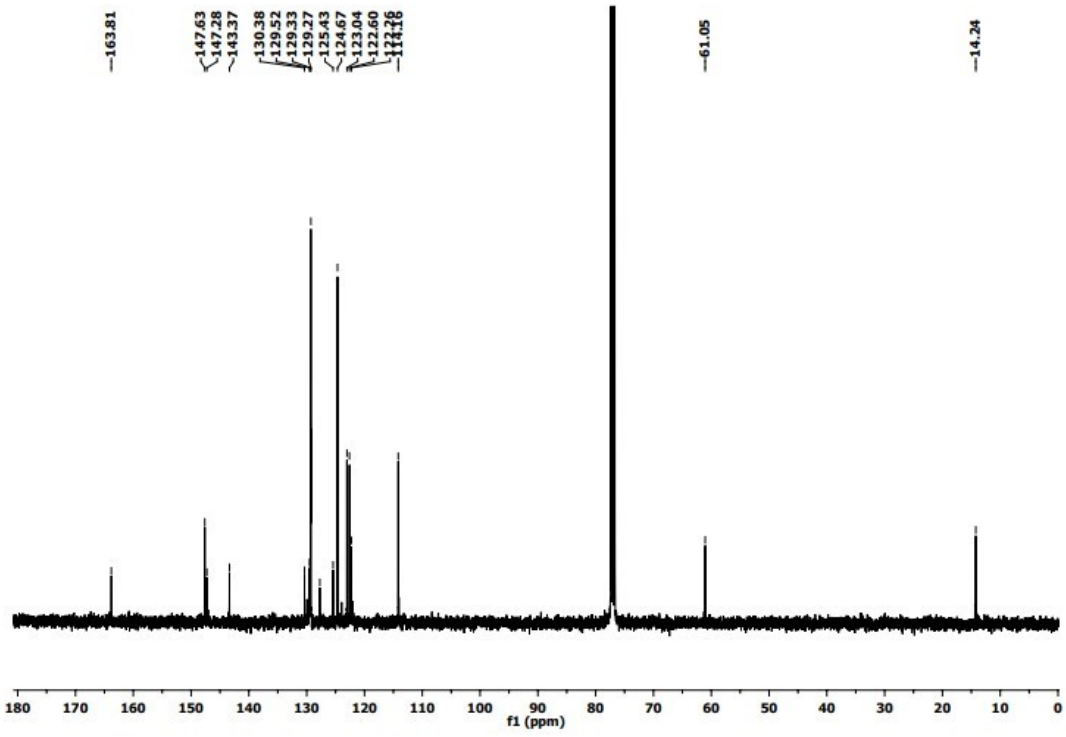

Fig. S8 ^{13}C NMR spectrum of 1.

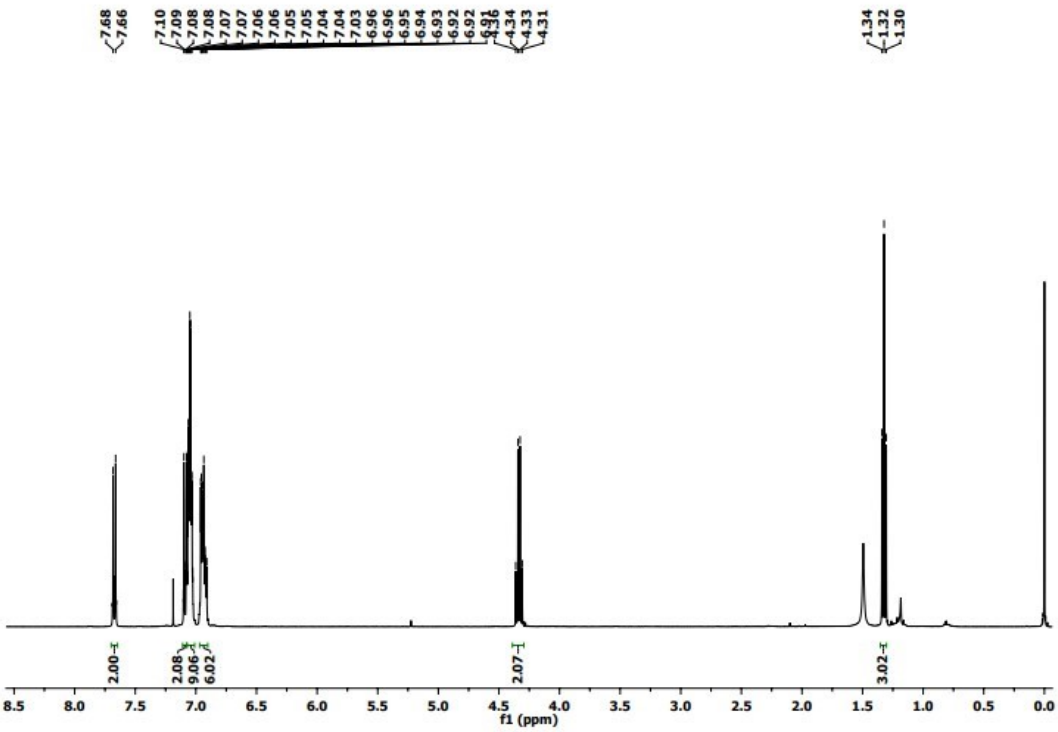

Fig. S9 ^{1}H NMR spectrum of 2.

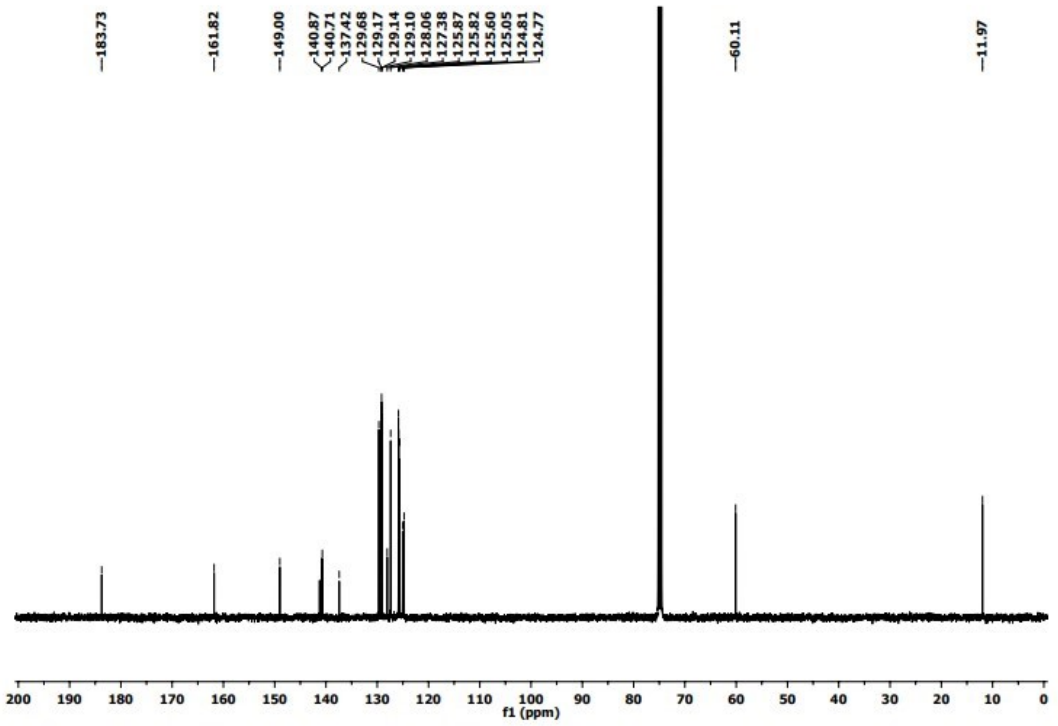

Fig. S10 ^{13}C NMR spectrum of 2.

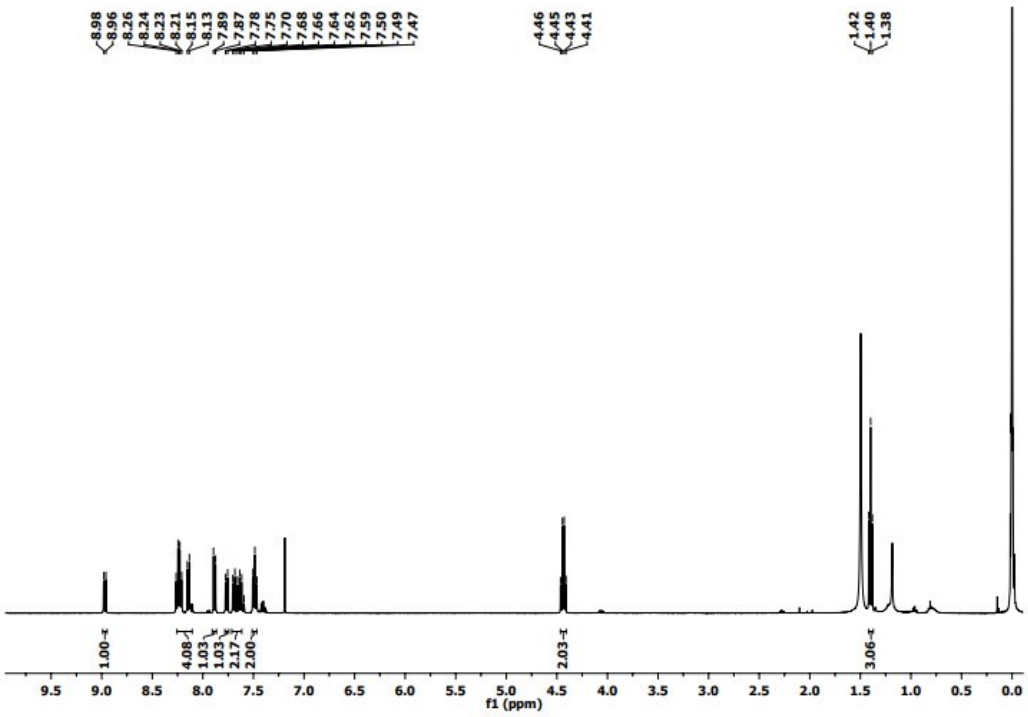

Fig. S11 ^{1}H NMR spectrum of 3.

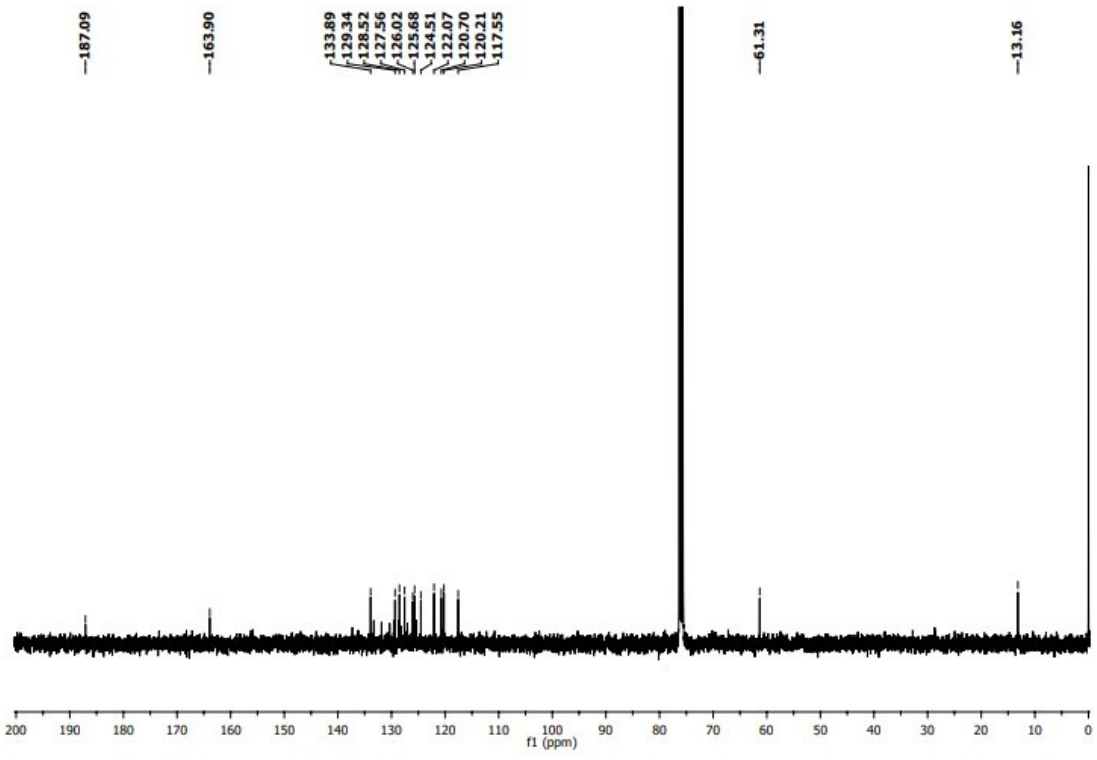

Fig. S12 ^{13}C NMR spectrum of 3.

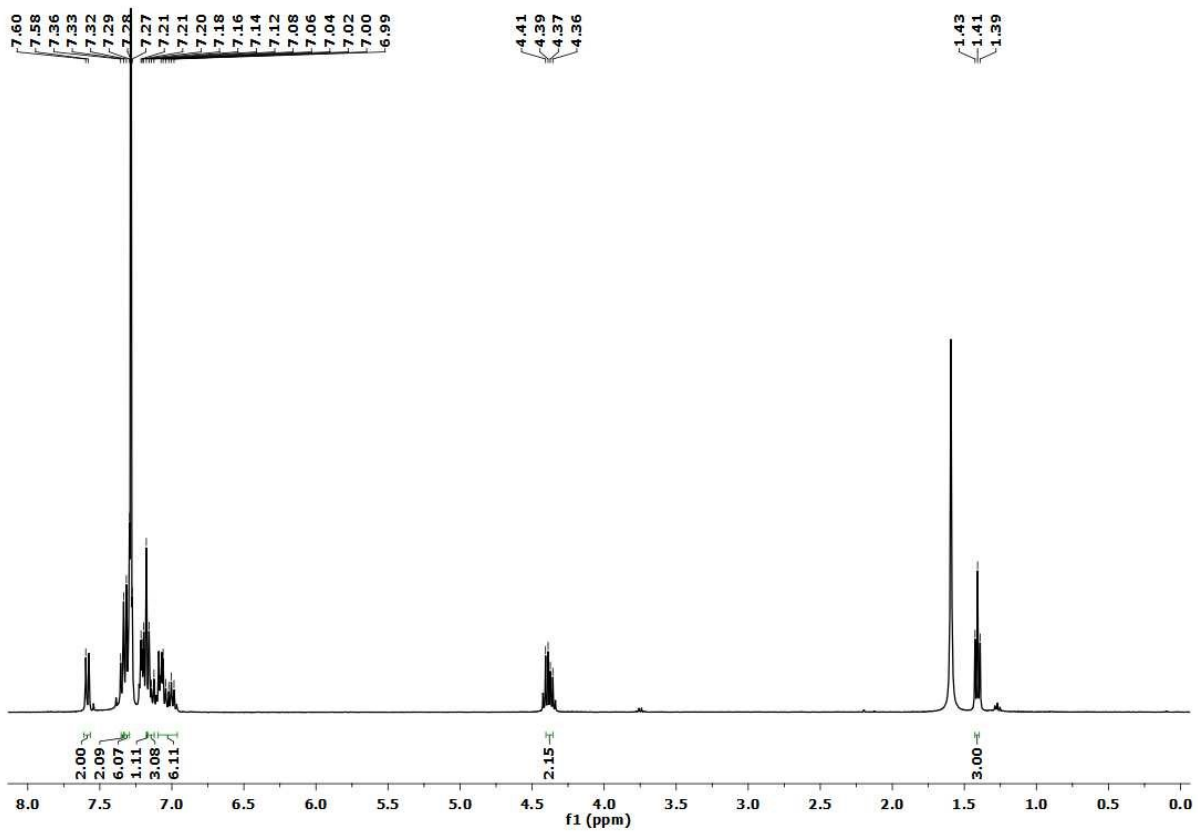

Fig. S13 ^{1}H NMR spectrum of TPA-PH.

Fig. S14 ^{13}C NMR spectrum of TPA-PH.

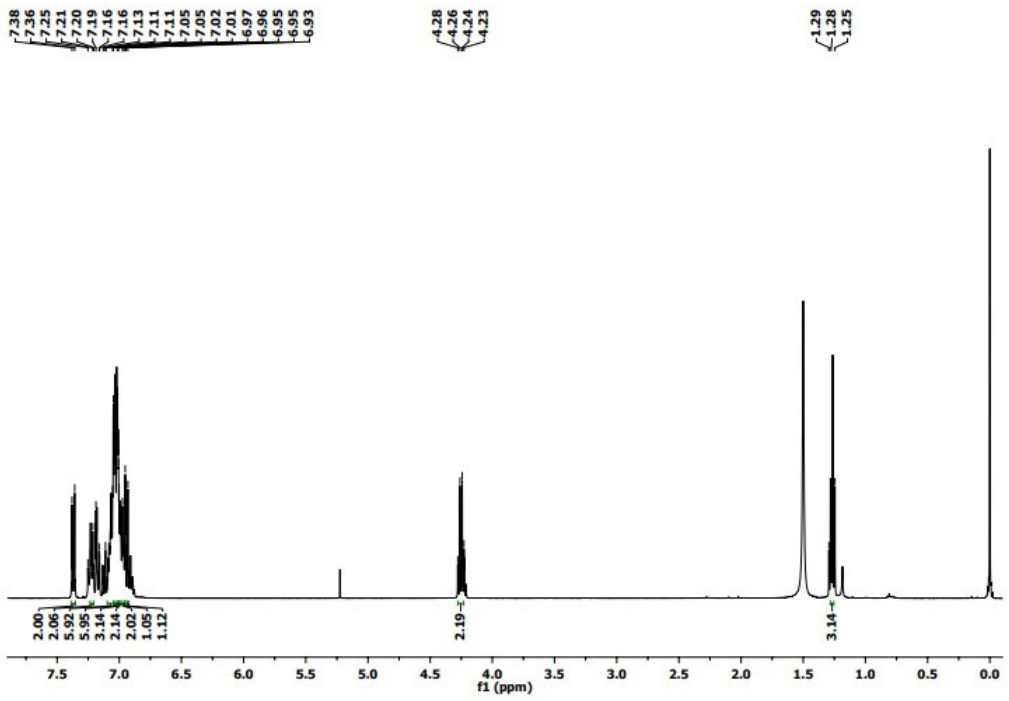

Fig. S15 ^{1}H NMR spectrum of TPE-PH.

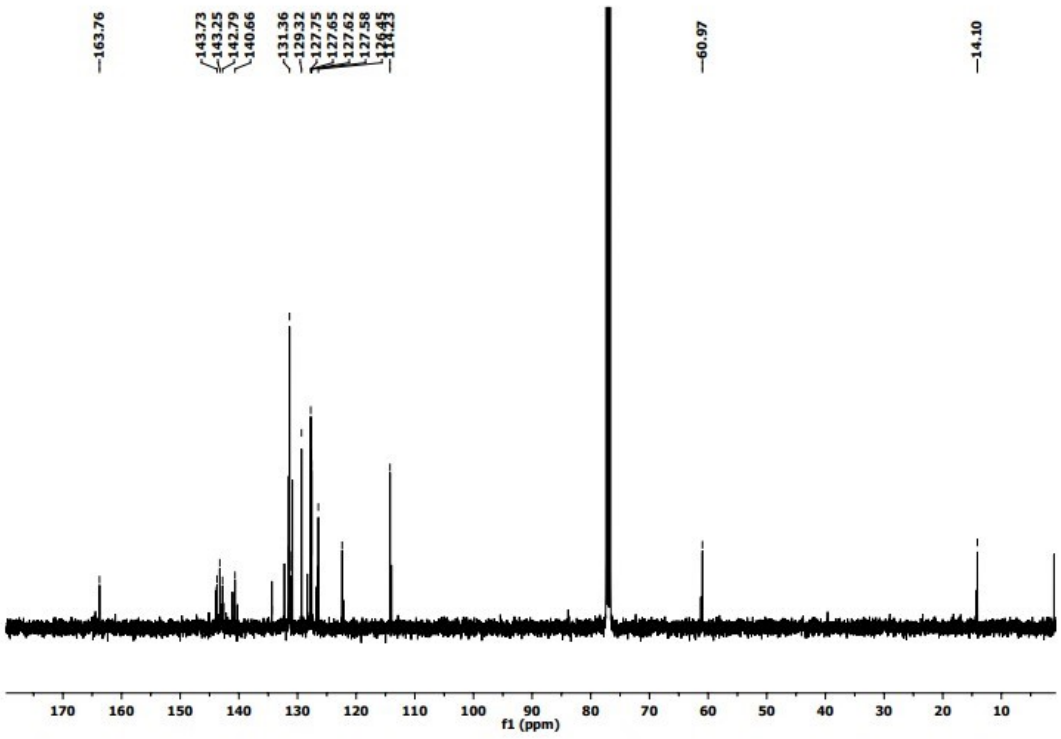

Fig. S16 ^{13}C NMR spectrum of TPE-PH.

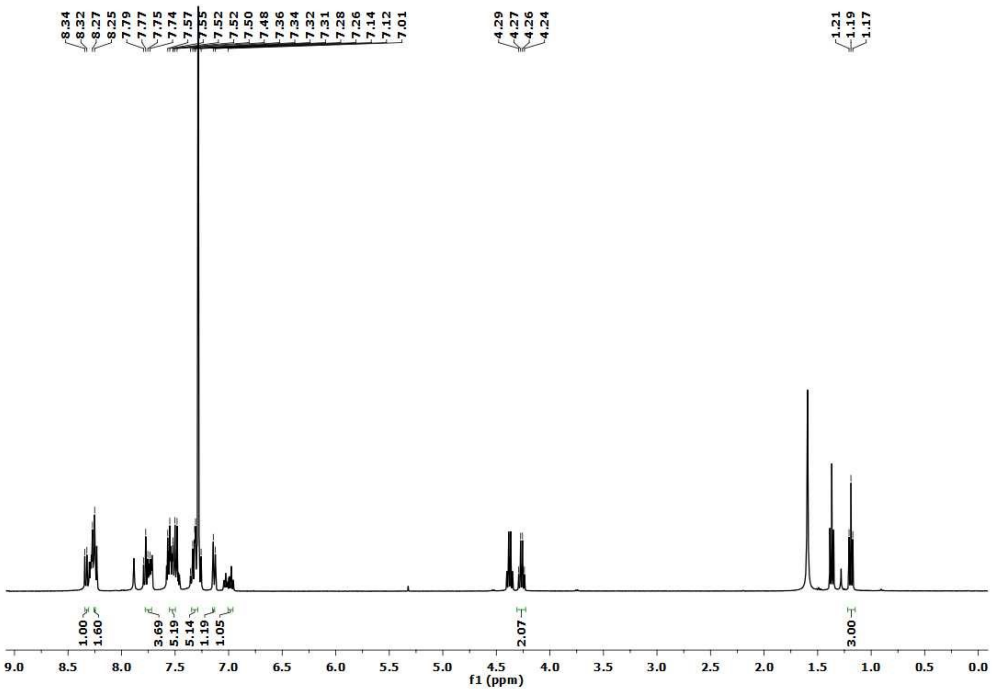

Fig. S17 ^{1}H NMR spectrum of PY-PH.

Fig. S18 ^{13}C NMR spectrum of PY-PH.

5. Mass Analysis

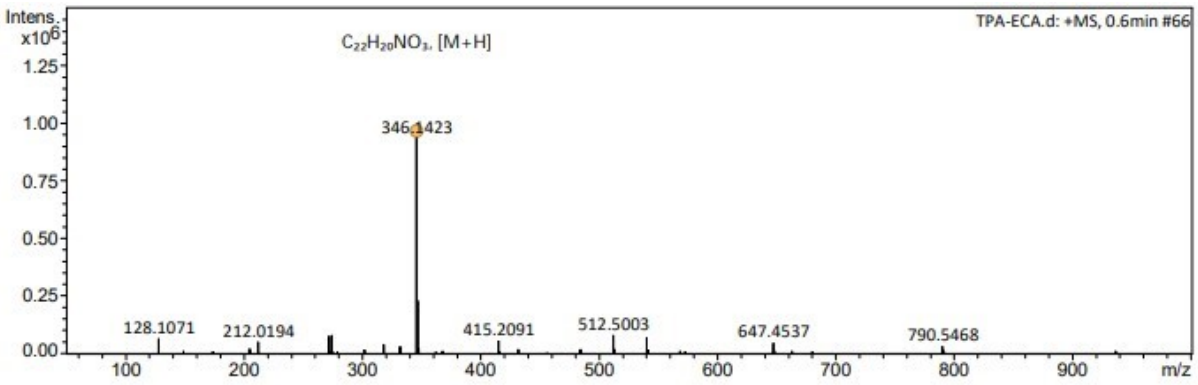

Fig. S19 Mass spectrum of 1.

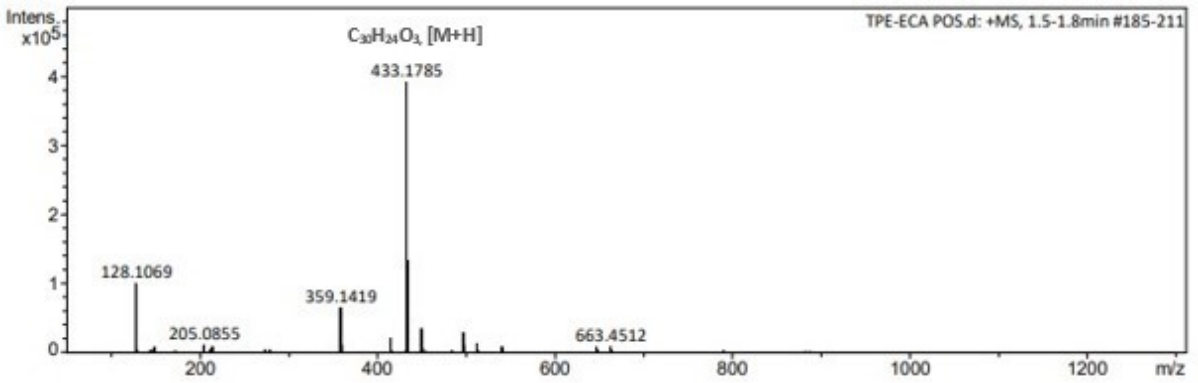

Fig. S20 Mass spectrum of 2.

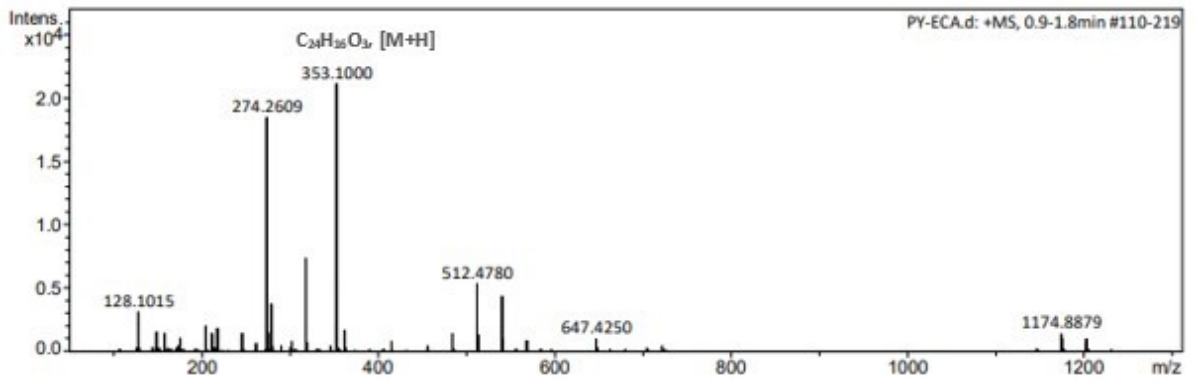

Fig. S21 Mass spectrum of 3.

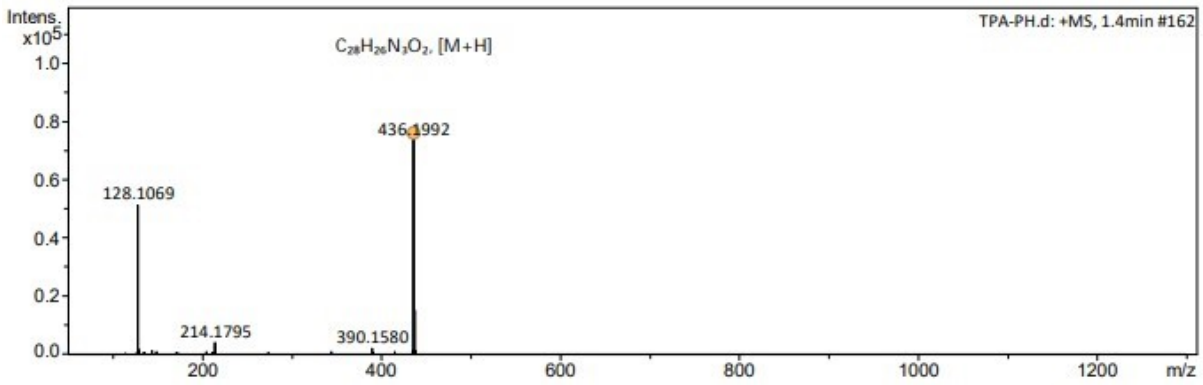

Fig. S22 Mass spectrum of TPA-PH.

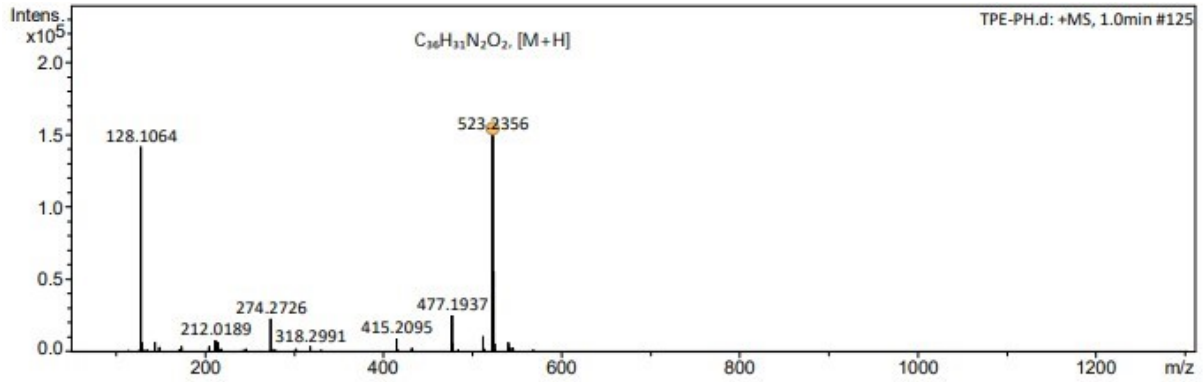

Fig. S23 Mass spectrum of TPE-PH.

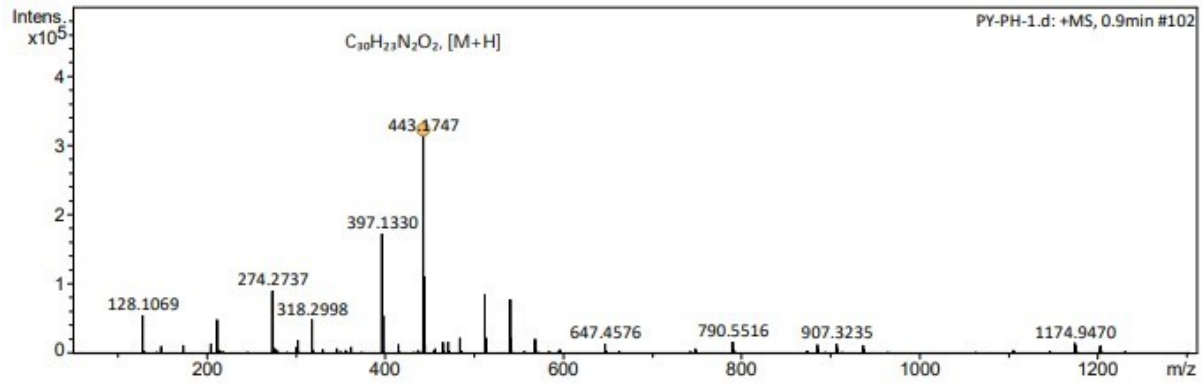

Fig. S24 Mass spectrum of PY-PH.

6. Single Crystal X-ray Crystallography Studies

Table S1. Crystal data and structural refinement for compounds **TPA-PH**, **TPE-PH** and **PY-PH**

Compound	TPA-PH	TPE-PH	PY-PH
Empirical formula	$C_{28}H_{25}N_3O_2$	$C_{36}H_{30}N_2O_2$	$C_{30}H_{22}N_2O_2$
Formula weight	435.51	522.62	442.49
T [K]	273(2)	273.15	273(2)
Crystal system	triclinic	triclinic	orthorhombic
Space group	*P-1*	*P-1*	*Pccn*
a, Å	9.8616(13)	9.2561(5)	40.059(3)
b, Å	9.9362(14)	12.7971(7)	12.3227(6)
c, Å	14.0691(19)	13.9549(10)	9.5736(6)
α, deg	83.174(4)	73.7090(10)	90
β, deg	73.214(3)	70.63	90
γ, deg	61.320(3)	68.80	90
Volume ($Å^3$)	1157.6(3)	1429.44(15)	4725.9(5)
Z	2	2	8
d_{calc} (mg/cm^3)	1.249	1.214	1.244
μ (mm^{-1})	0.080	0.075	0.078
F(000)	460.0	552.0	1856.0
Crystal size/mm^3	0.36 × 0.34 × 0.17	0.18 × 0.14 × 0.03	0.34 × 0.18 × 0.02
2Θ range for data collection/°	4.674 to 56.588	5.094 to 56.71	4.066 to 56.682
Reflections collected	25197	14688	62009
Data/restraints/parameters	5680/0/299	4950/6/366	5896/3/318
Goodness-of-fit on F^2	1.063	1.005	1.051
R [I>2σ (I)]	$R_1 = 0.0510$ $wR_2 = 0.1395$	$R_1 = 0.0653$ $wR_2 = 0.1783$	$R_1 = 0.0628$ $wR_2 = 0.2341$
R [all data]	$R_1 = 0.0593$ $wR_2 = 0.1476$	$R_1 = 0.1269$ $wR_2 = 0.2191$	$R_1 = 0.1405$ $wR_2 = 0.2469$
Largest diff. Peak/hole [e $Å^{-3}$]	0.25/-0.17	0.24/-0.13	0.32/-0.17
CCDC number	2223713	2223714	2223715

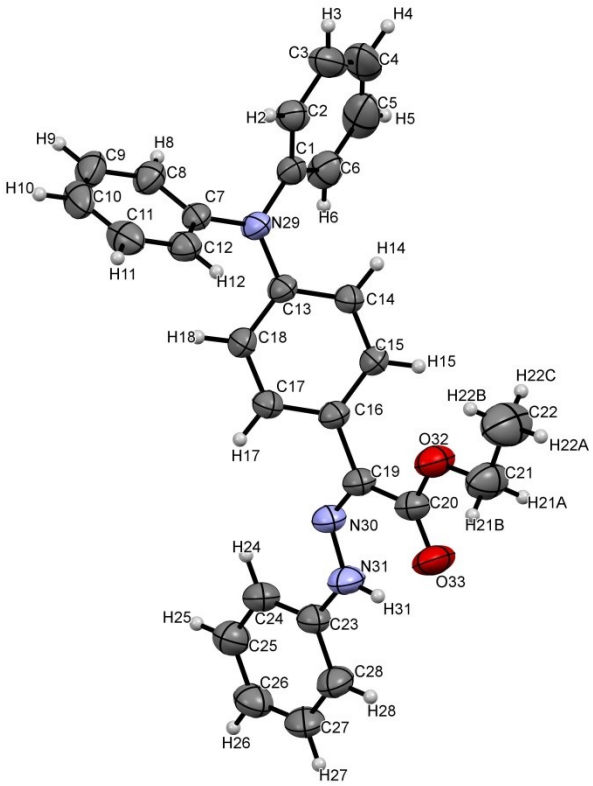

Fig. S25 ORTEP diagram of TPA-PH.

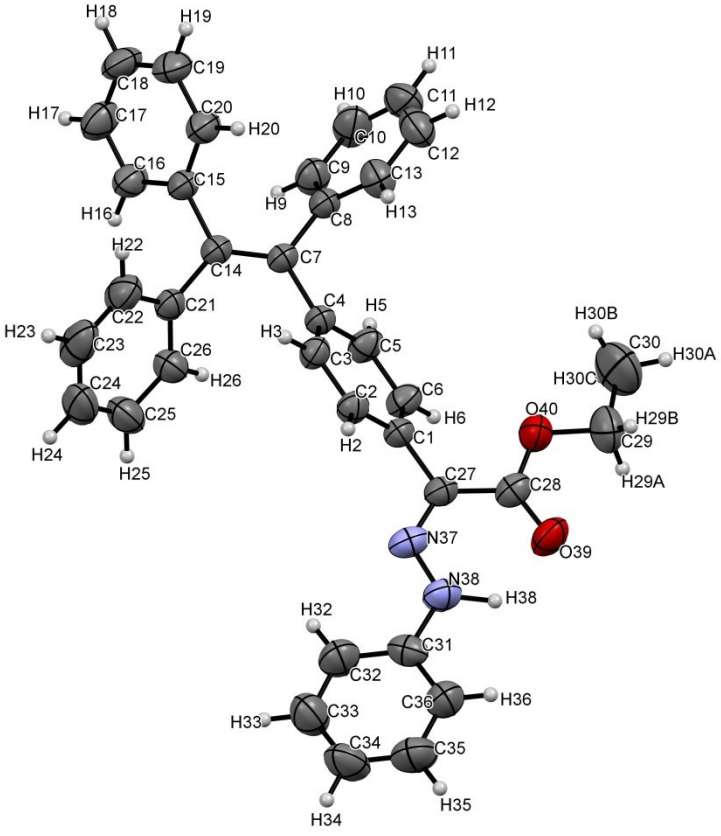

Fig. S26 ORTEP diagram of TPE-PH.

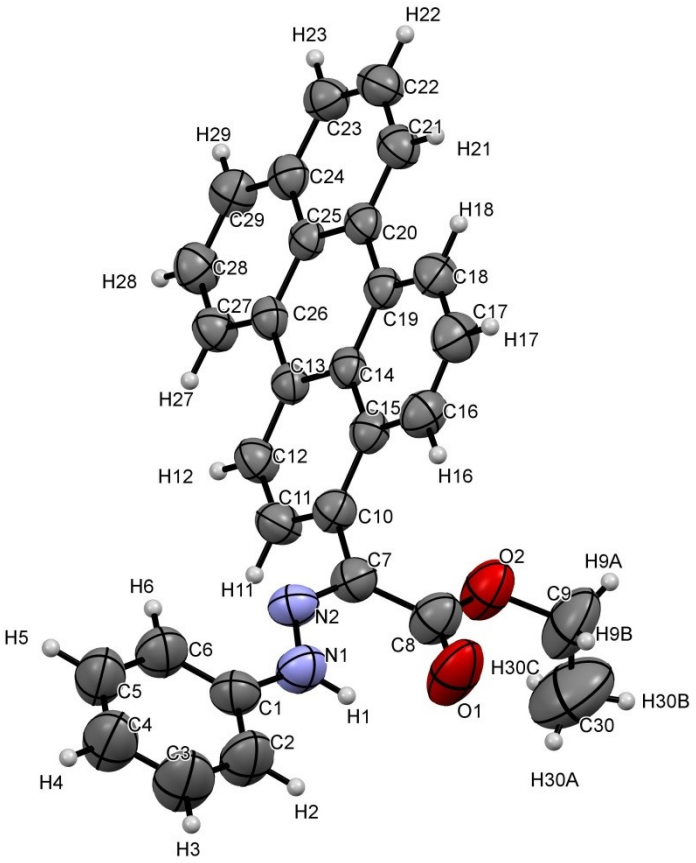

Fig. S27 ORTEP diagram of PY-PH.

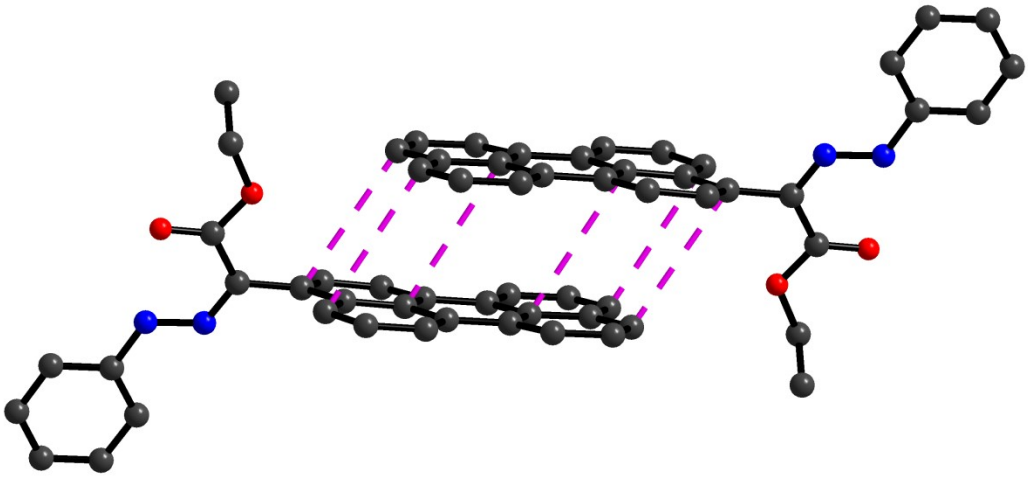

Fig. S28 The π–π stacking dimer formed in TPA-PH.

7. Aggregation-induced emission (AIE) studies

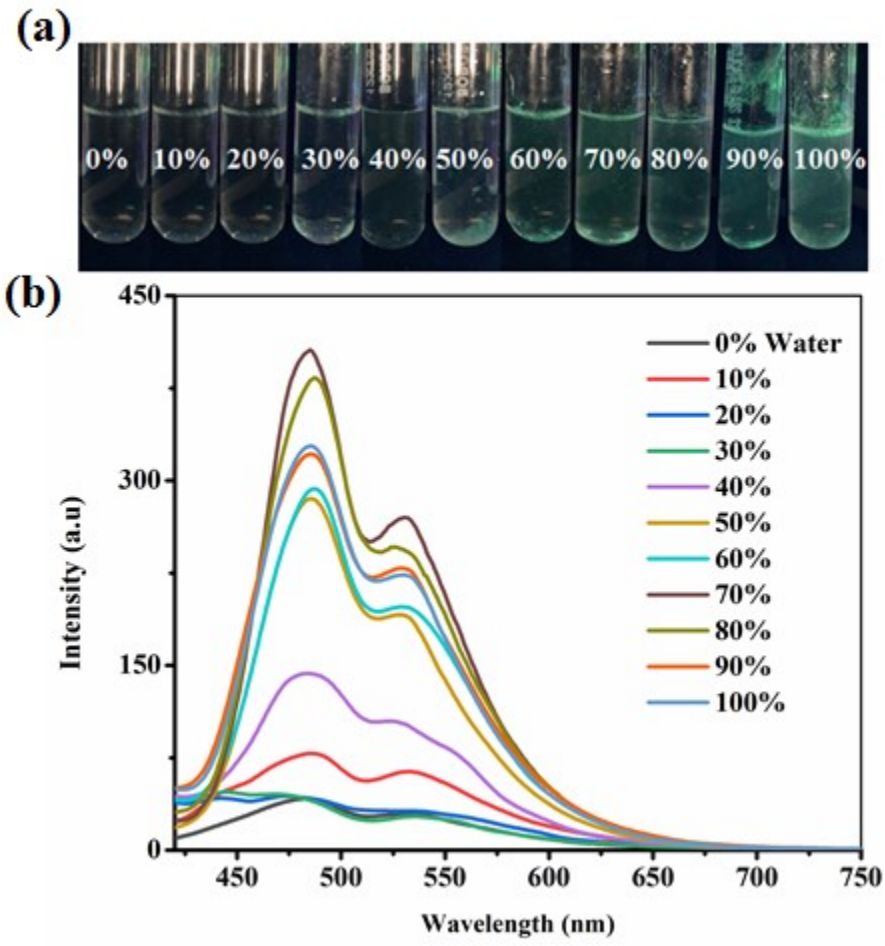

Fig. S29 (a) Photographs of TPE-PH in THF–H_2O mixture (f_w = 0 to ~100 %) under 365 nm UV light. (b) Emission spectra of TPE-PH in THF–H_2O mixtures (1.0×10^{-5} M) with different H_2O fractions (0 to ~100%) at room temperature.

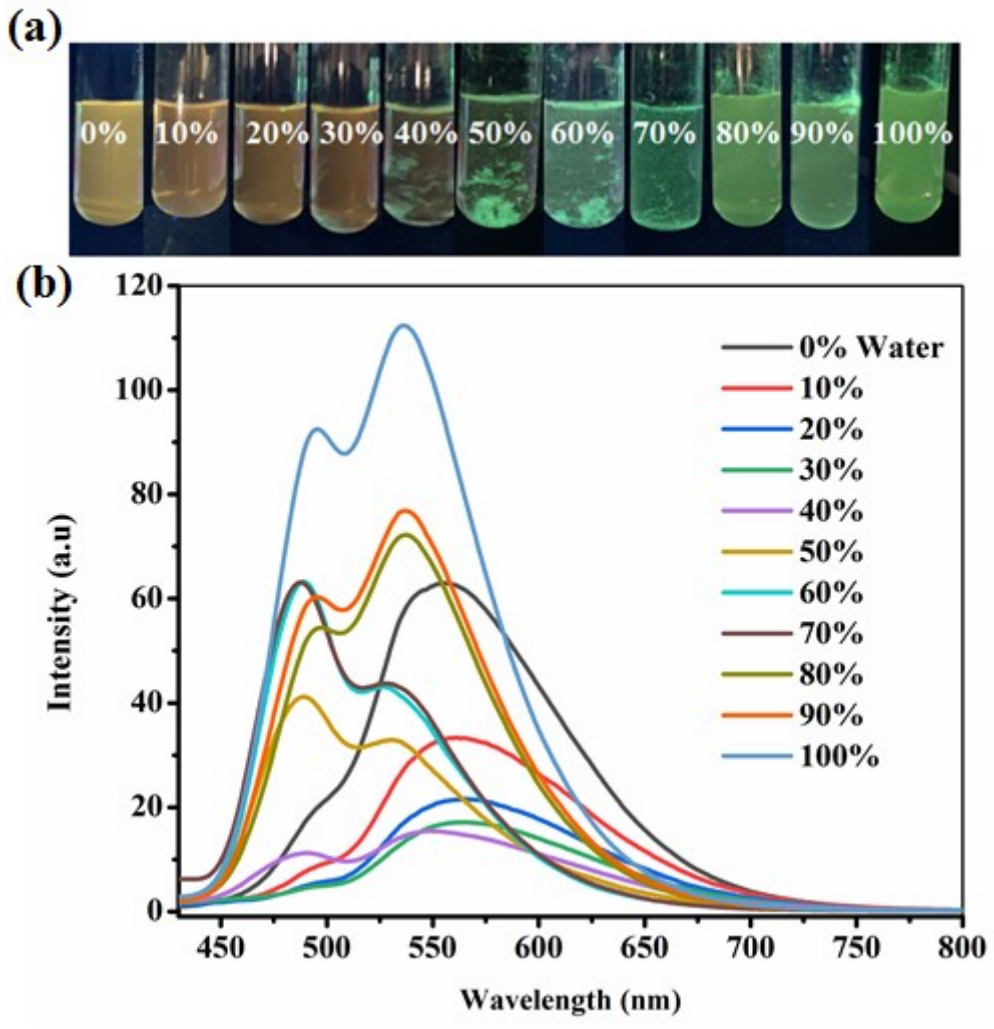

Fig. S30 (a) Photographs of TPA-PH in THF–H_2O mixture (f_w = 0 to ~100 %) under 365 nm UV light. (b) Emission spectra of TPA-PH in THF–H_2O mixtures (1.0×10^{-5} M) with different H_2O fractions (0 to ~100%) at room temperature.

8. Photophysical studies

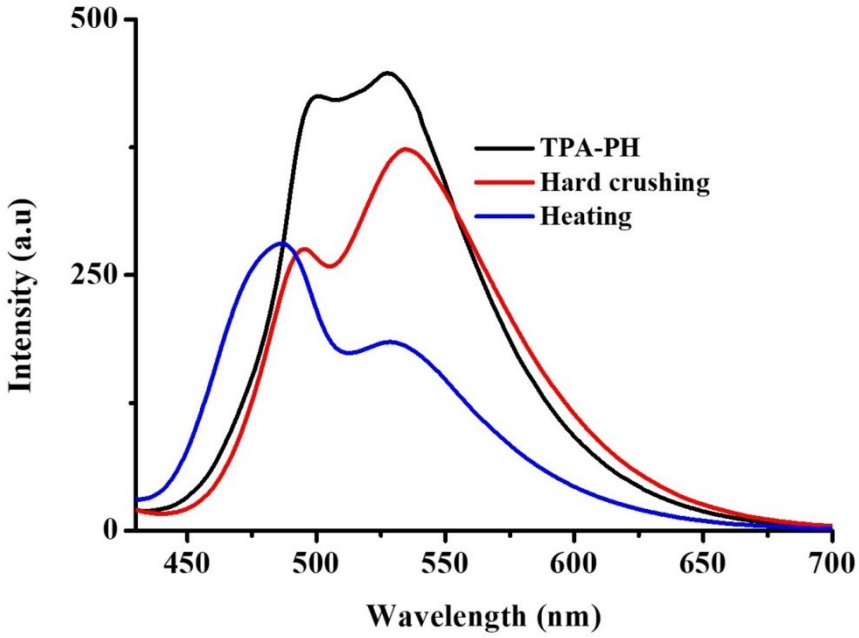

Fig. S31 Mechanofluorochromism of TPA-PH.

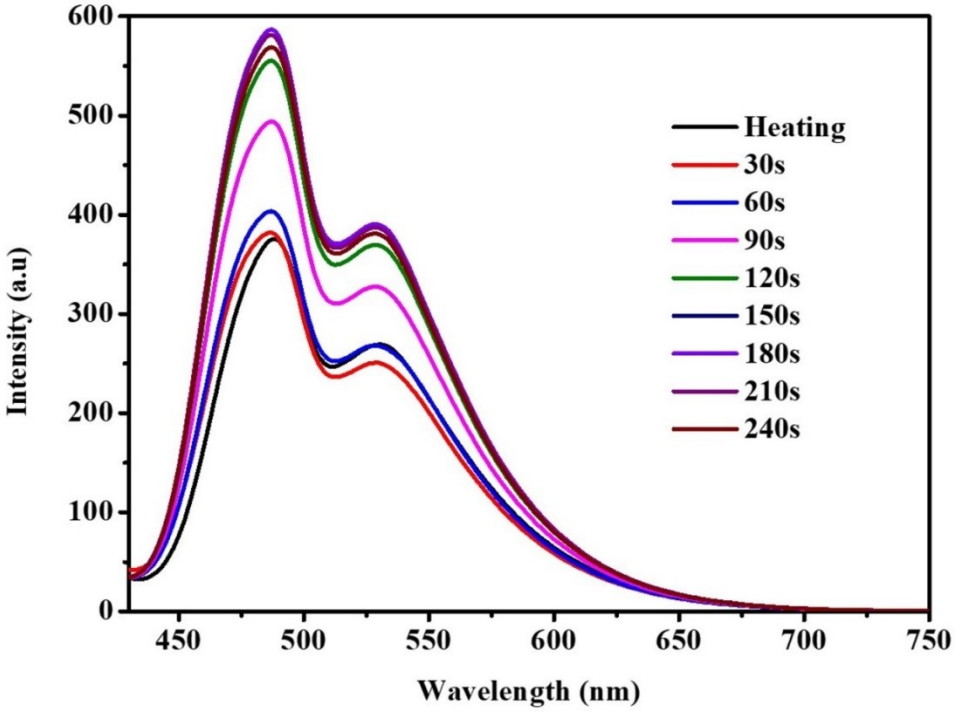

Fig. S32 Fluorescence change upon cooling of heated TPA-PH showed clear increase of fluorescence intensity.

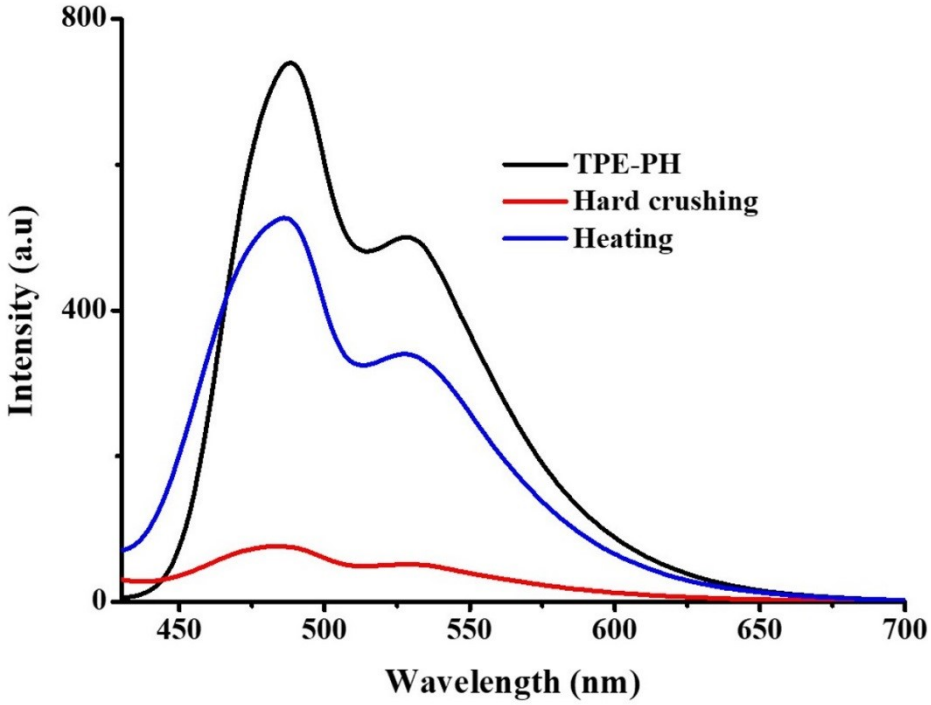

Fig. S33 Mechanofluorochromism of TPE-PH.

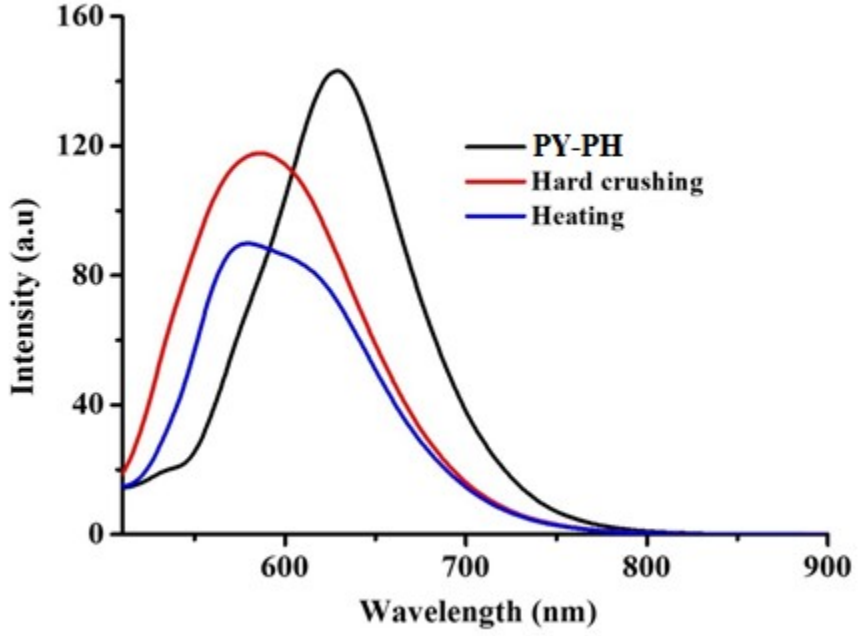

Fig. S34 Mechanofluorochromism of PY-PH.

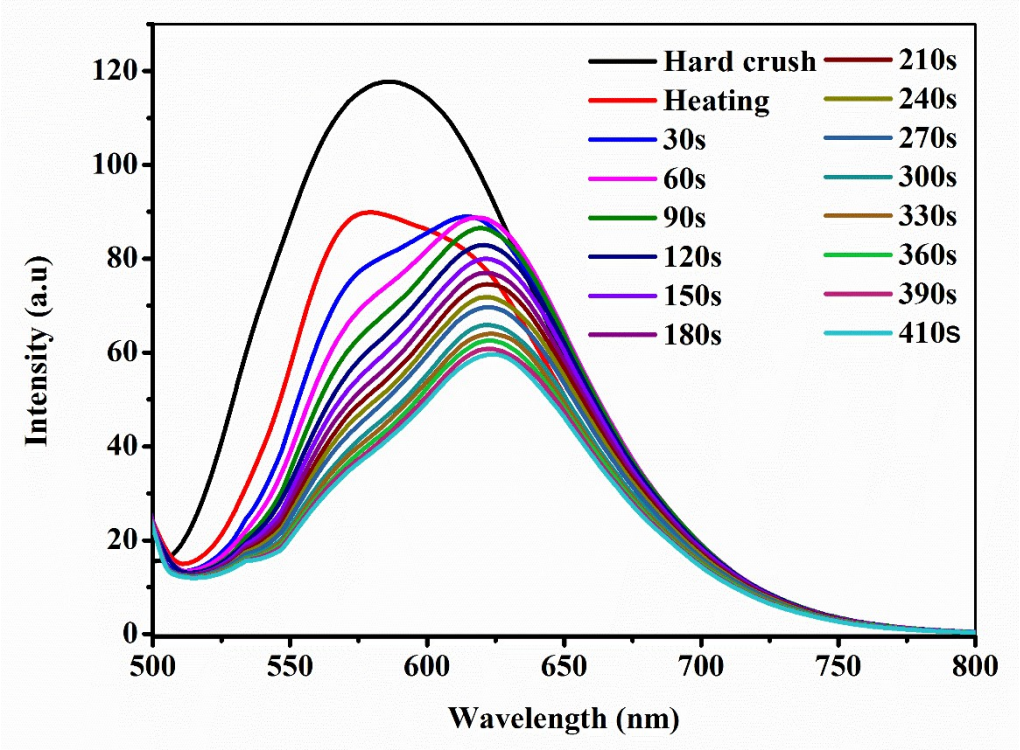

Fig. S35 Irreversible fluorescence switching upon crushing/heating of PY-PH.

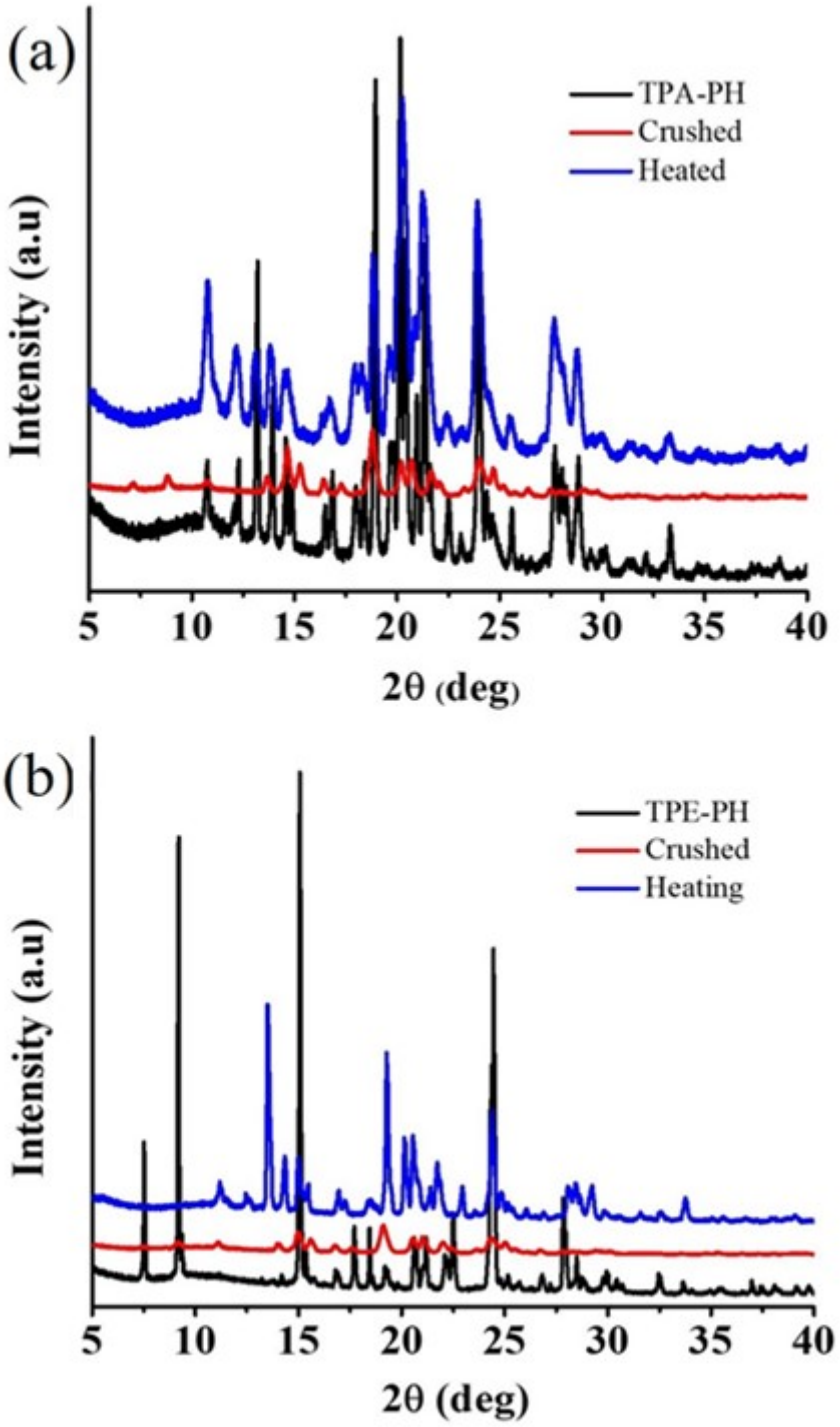

Fig. S36 PXRD patterns of (a) TPA-PH and (b) TPE-PH at different state mechanofluorochromic studies,

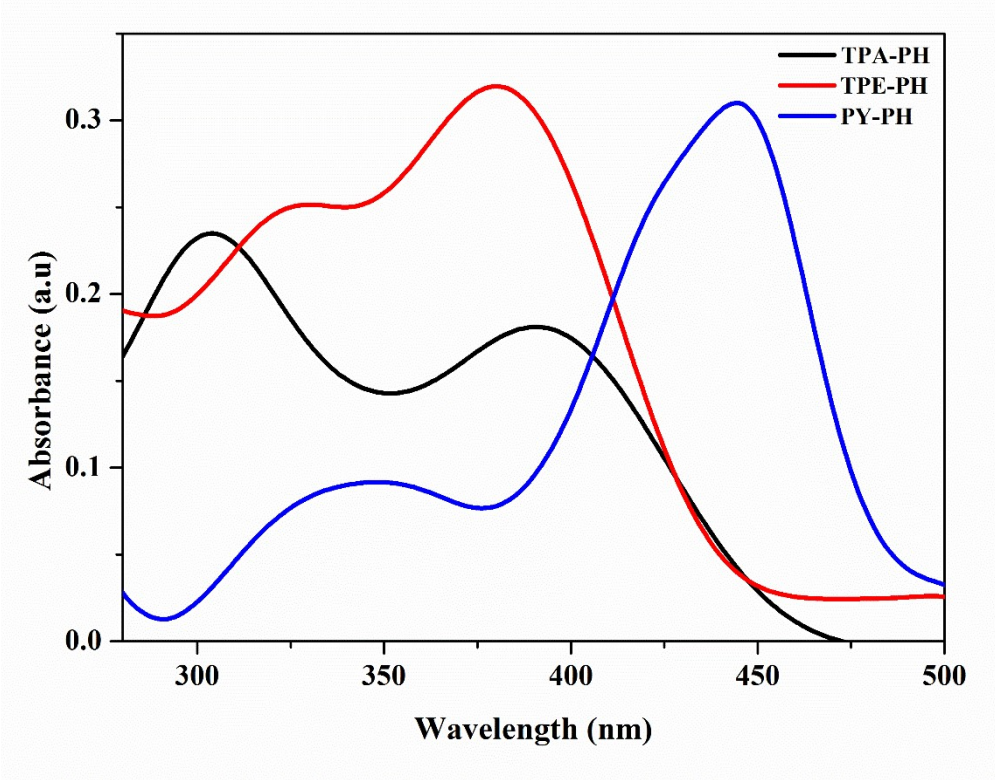

Fig. S37 The absorption spectra of **TPA-PH**, **TPE-PH** and **PY-PH** measured in $CHCl_3$ (1.0×10^{-5} M) at room temperature.

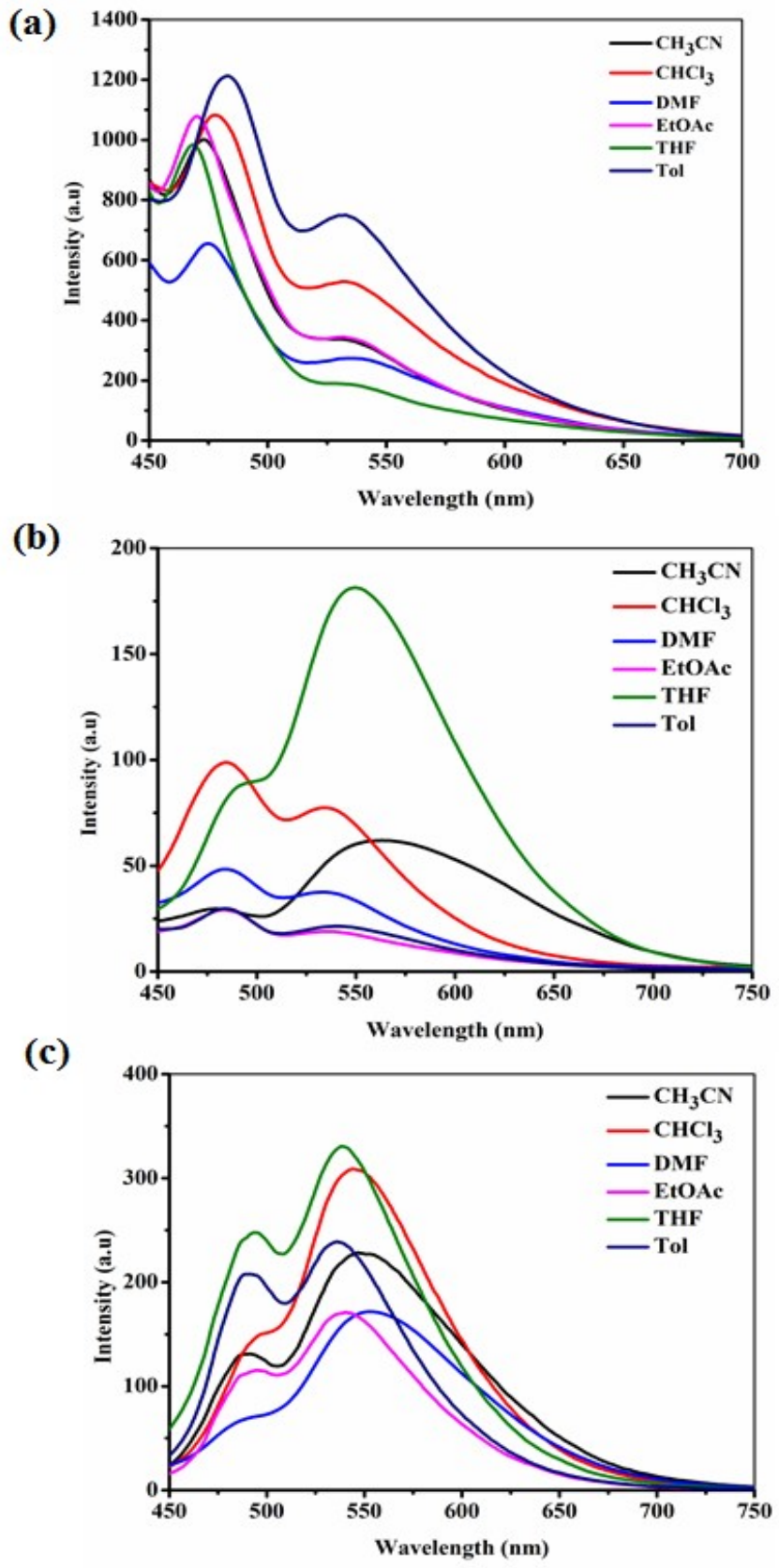

Fig. S38 Solvatochromic studies of (a) PY-PH, (b) TPE-PH and (c) TPA-PH in different solvents.

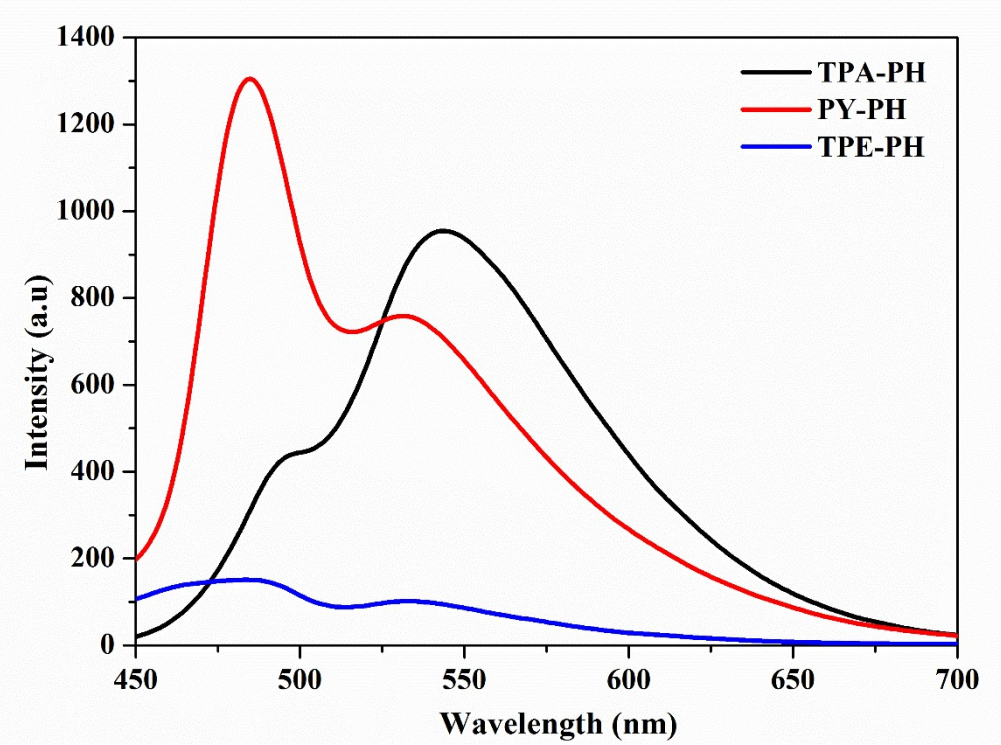

Fig. S39 The fluorescence spectra of **TPA-PH**, **TPE-PH** and **PY-PH** measured in $CHCl_3$ (1.0×10^{-5} M) at room temperature.

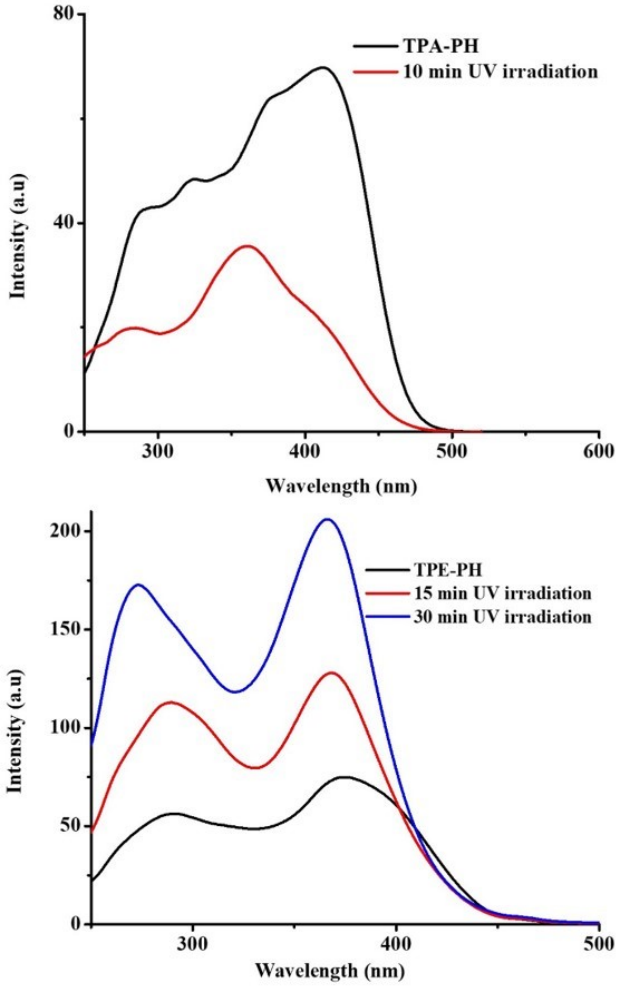

Fig. S40 Excitation spectra for **TPA-PH** and **TPE-PH** measured in $CHCl_3$ (1.0×10^{-5} M) at room temperature.

Table S2. The photophysical properties of **TPA-PH**, **TPE-PH** and **PY-PH** measured in $CHCl_3$ solution at room temperature. Quantum yield measured with respect to quinine sulphate standard.

Compound	$\lambda_{max\ abs}$ (nm)	$\lambda_{max\ em}$ (nm)[a]	$\lambda_{max\ em}$ (nm)[b]	Φ_f[a]	Φ_f[b]
TPA-PH	304 (π–π*), 390 (ICT)	497, 544	479, 537	0.23	0.15
TPE-PH	326 (π–π*), 380 (ICT)	477, 532	460, 532	0.02	0.21
PY-PH	348 (π–π*), 444 (ICT)	484, 532	495, 541	0.34	0.24

[a)]before irradiation of light
[b)]after irradiation of light

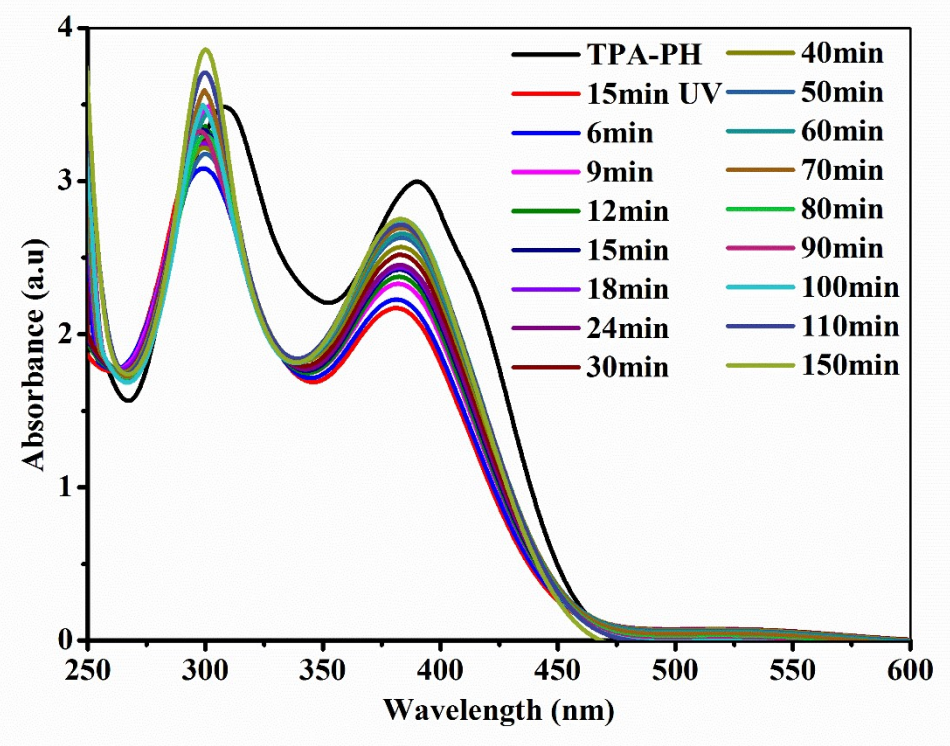

Fig. S41 Absorption changes for reversible Z↔E photoisomerization of TPA-PH under irradiation of light in $CHCl_3$ (1.0×10^{-5} mol L^{-1}) in different time.

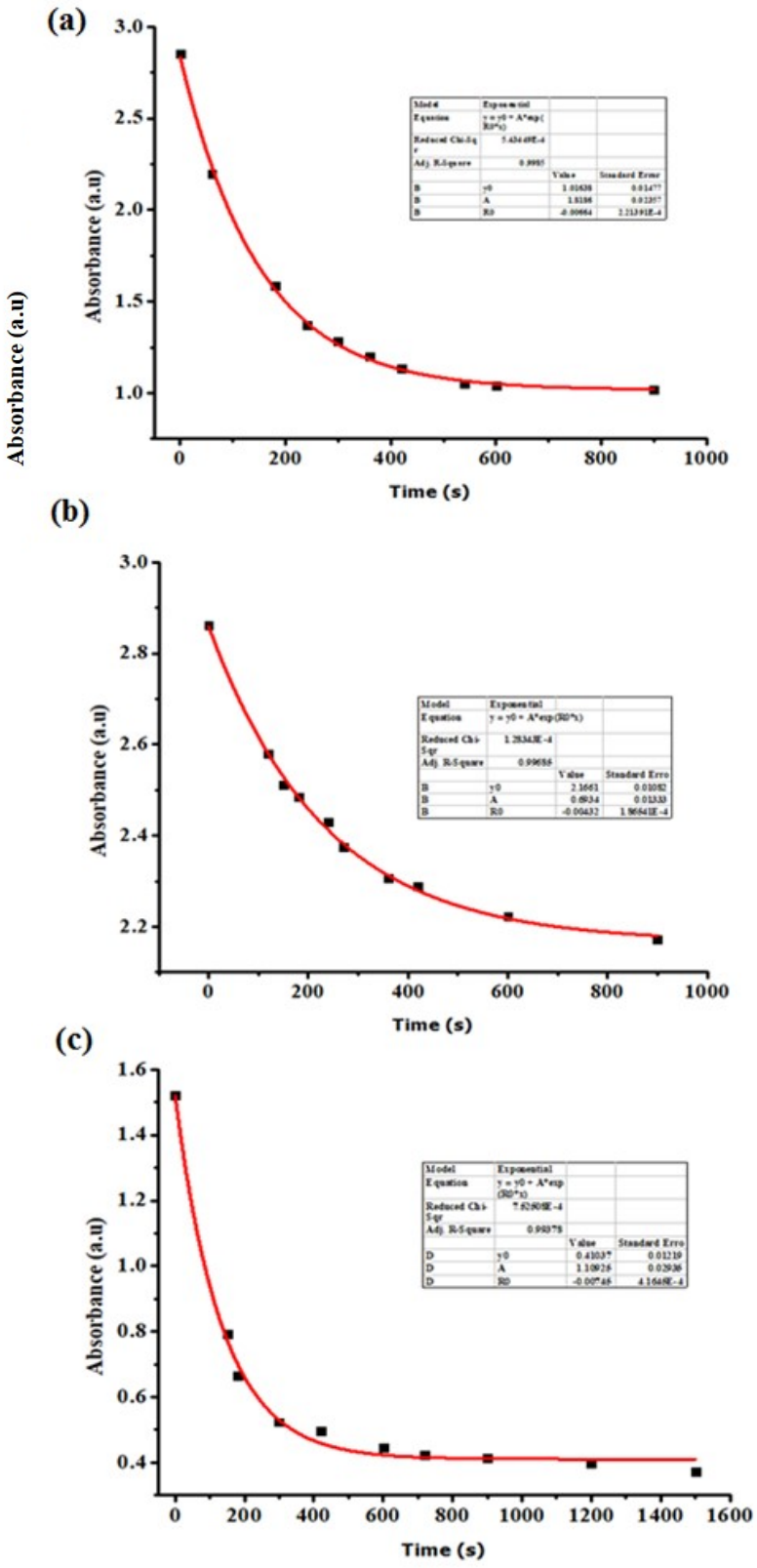

Fig. S42 The plot for calculation of quantum yield for Z→E photoisomerization (irradiation at 365 nm) of (a) TPA-PH, (b) TPE-PH and (c) PY-PH in $CHCl_3$ (1×10^{-5} M) using the absorbance (λ_{max}) of Z isomer as a function of time.

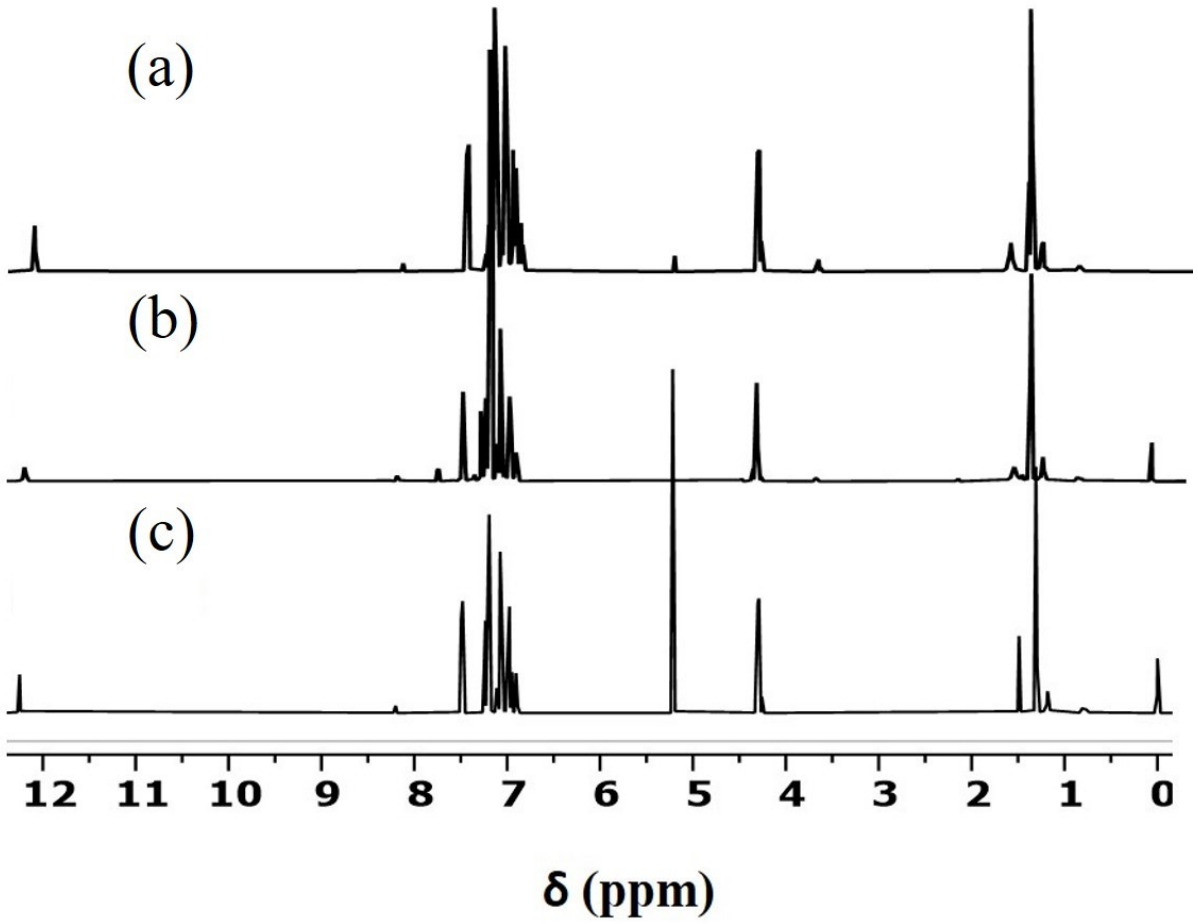

Fig. S43 ^{1}H NMR spectrum of TPA-PH. (a) before irradiation of light, (b) after irradiation of light, (c) after complete reversibility under the absence of light.

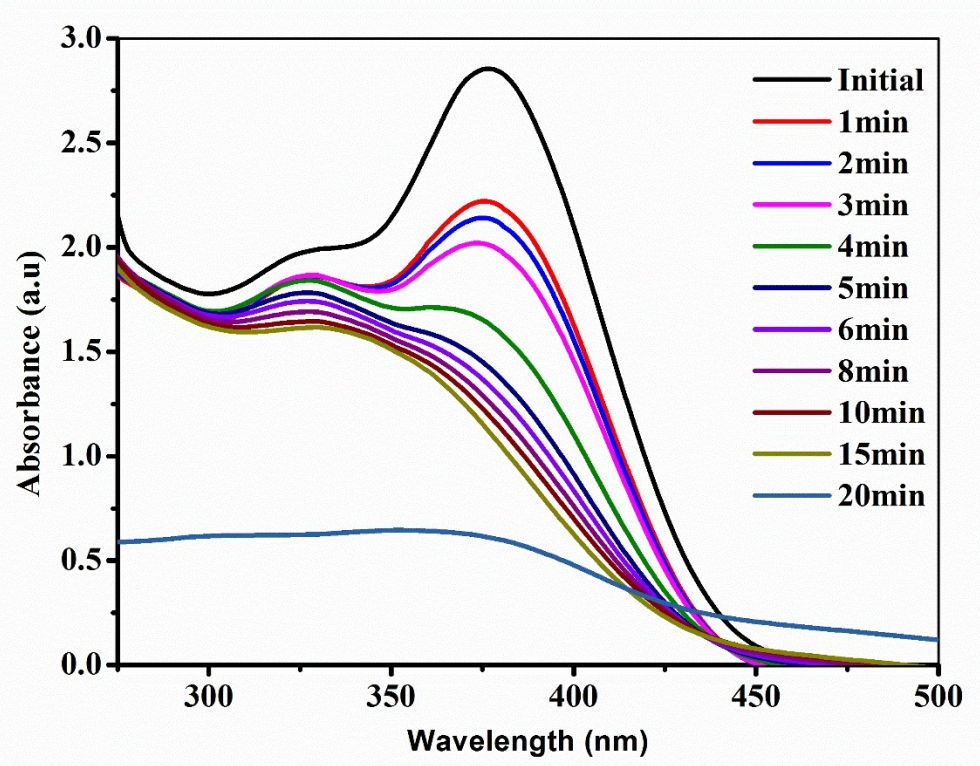

Fig. S44 Absorption changes for reversible Z↔E photoisomerization of TPE-PH under irradiation of light in $CHCl_3$ (1.0×10^{-5} mol L^{-1}) in different time.

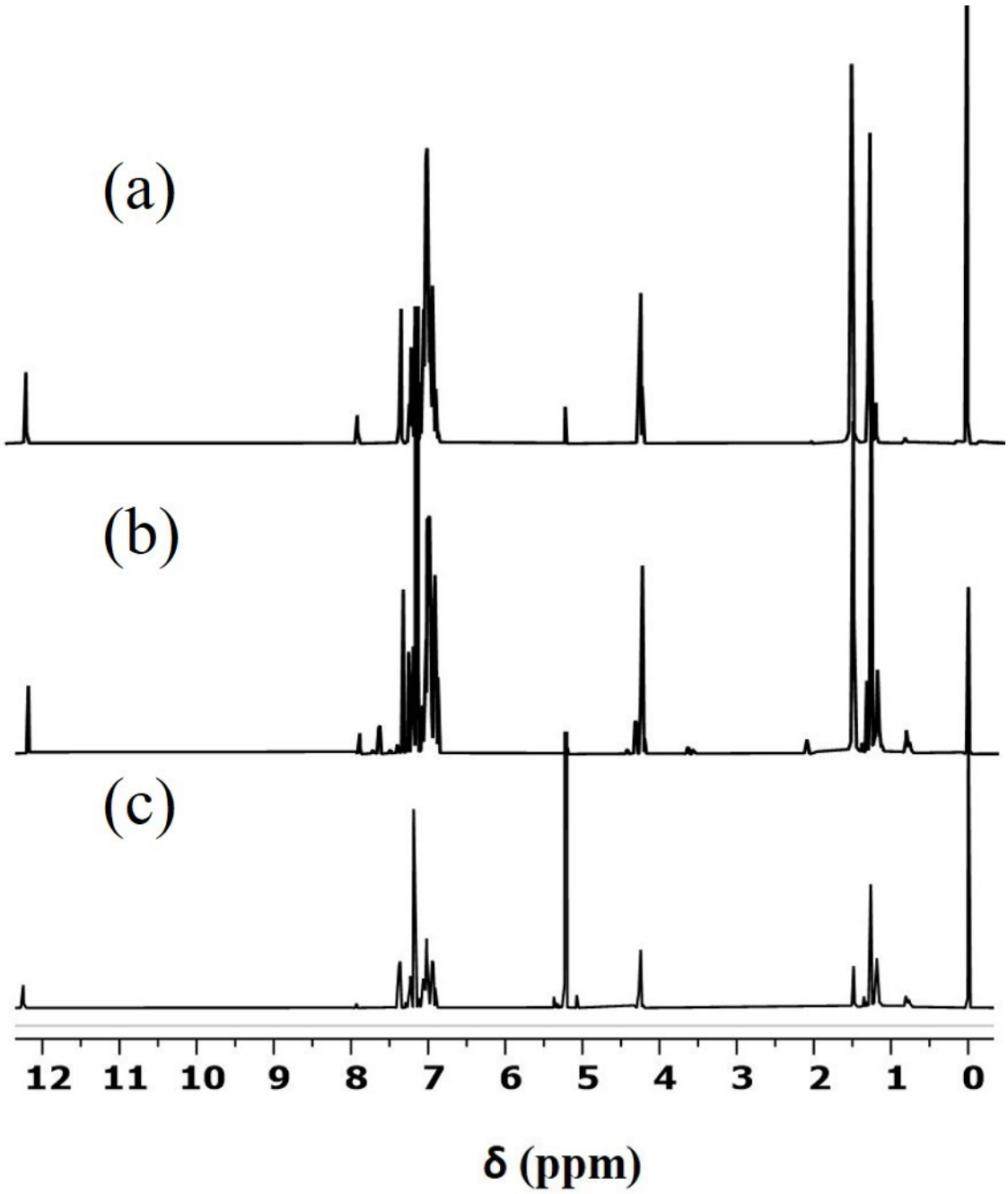

Fig. S45. ^{1}H NMR spectrum of TPE-PH. (a) before irradiation of light, (b) after irradiation of light, (c) after complete reversibility under the absence of light.

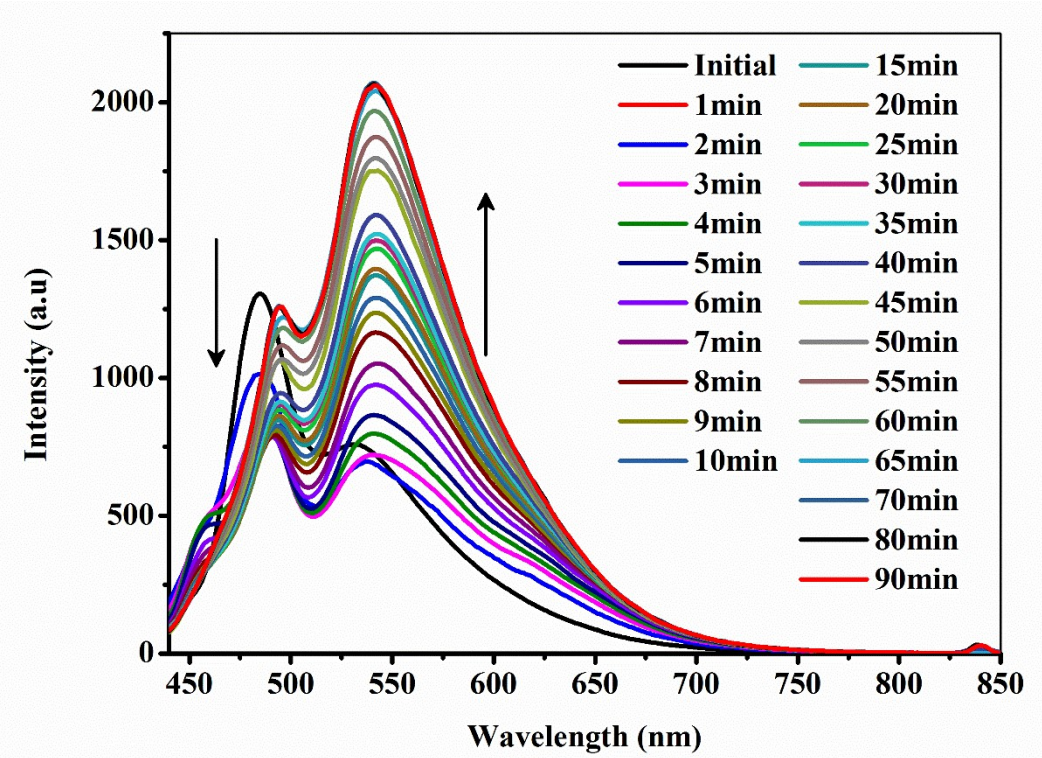

Fig. S46 *Z*→*E* photoisomerization of **PY-PH** upon irradiation of light in $CHCl_3$ (1.0×10^{-5} M)

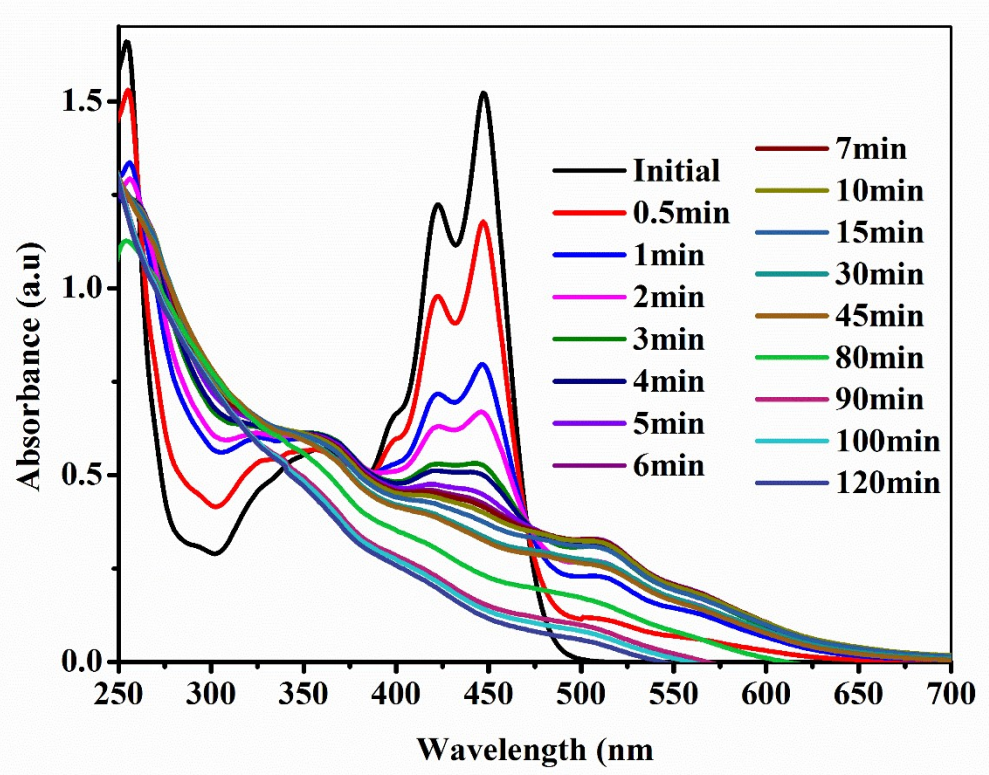

Fig. S47 Absorption changes for irreversible Z↔E photoisomerization of PY-PH under irradiation of light in $CHCl_3$ (1.0×10^{-5} mol L^{-1}) in different time.

(a)

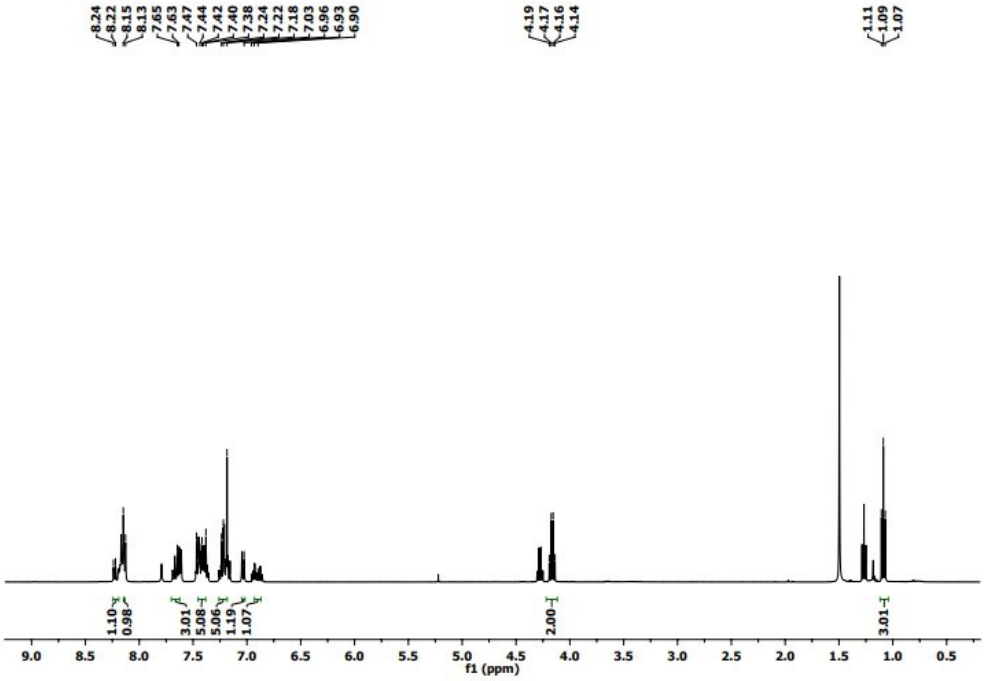

(b)

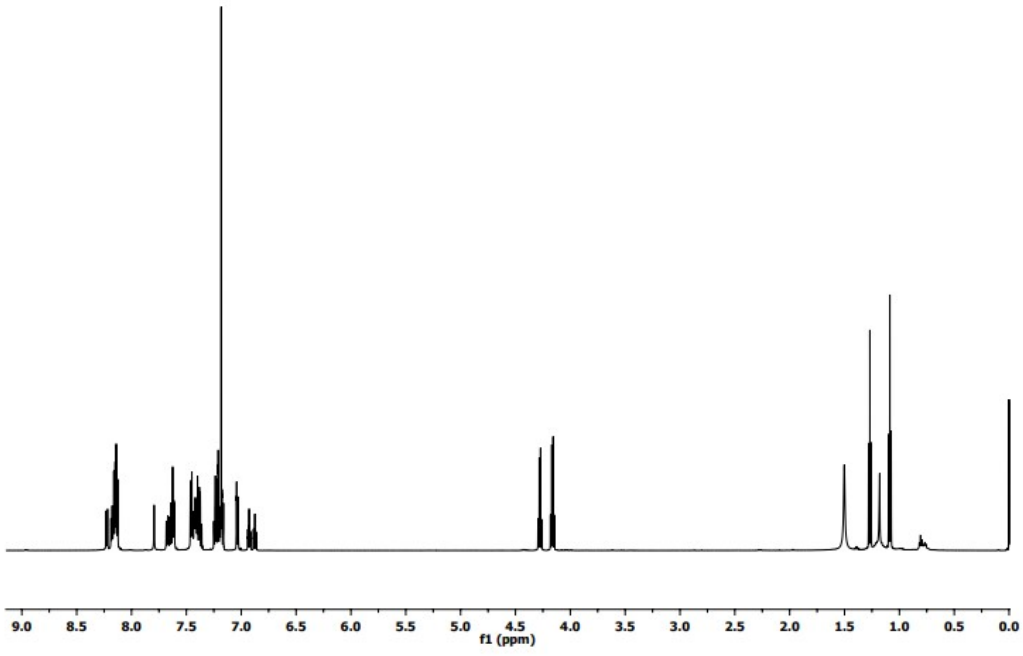

Fig. S48 ^{1}H NMR spectrum of PY-PH. (a) before irradiation of light. (b) After irradiation of light.

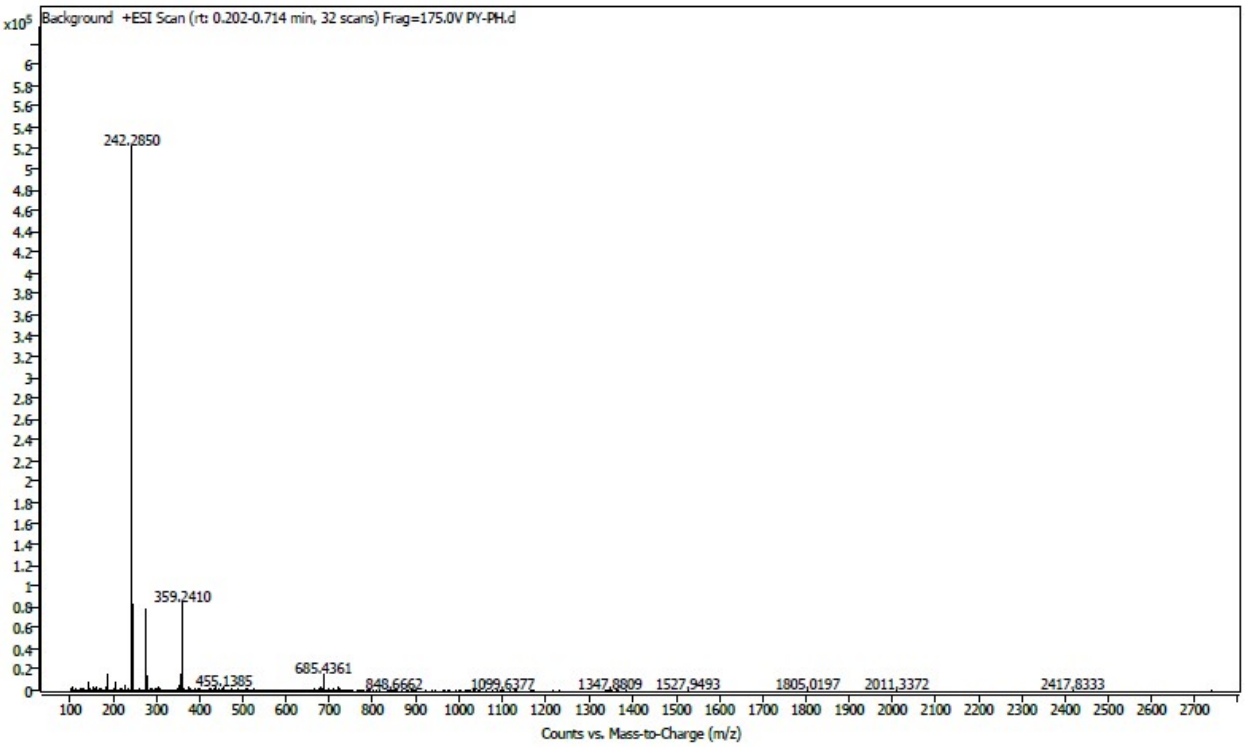

Fig. S49 Mass spectrum of PY-PH after irradiation of light.

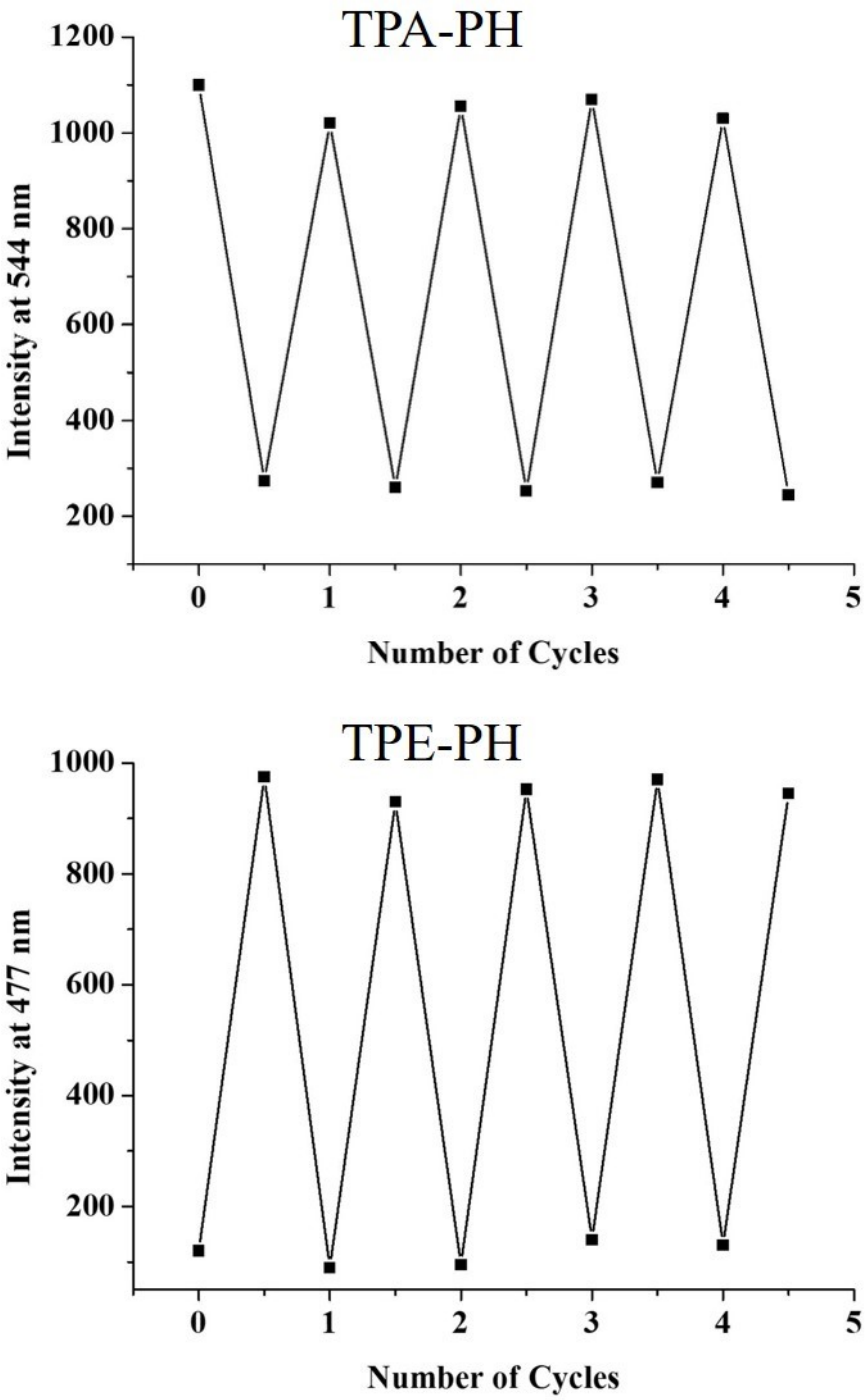

Fig. S50 Reversible fluorescence photoswitching cycles of TPA-PH and TPE-PH upon alternative irradiation of 365 nm UV and UV light off.

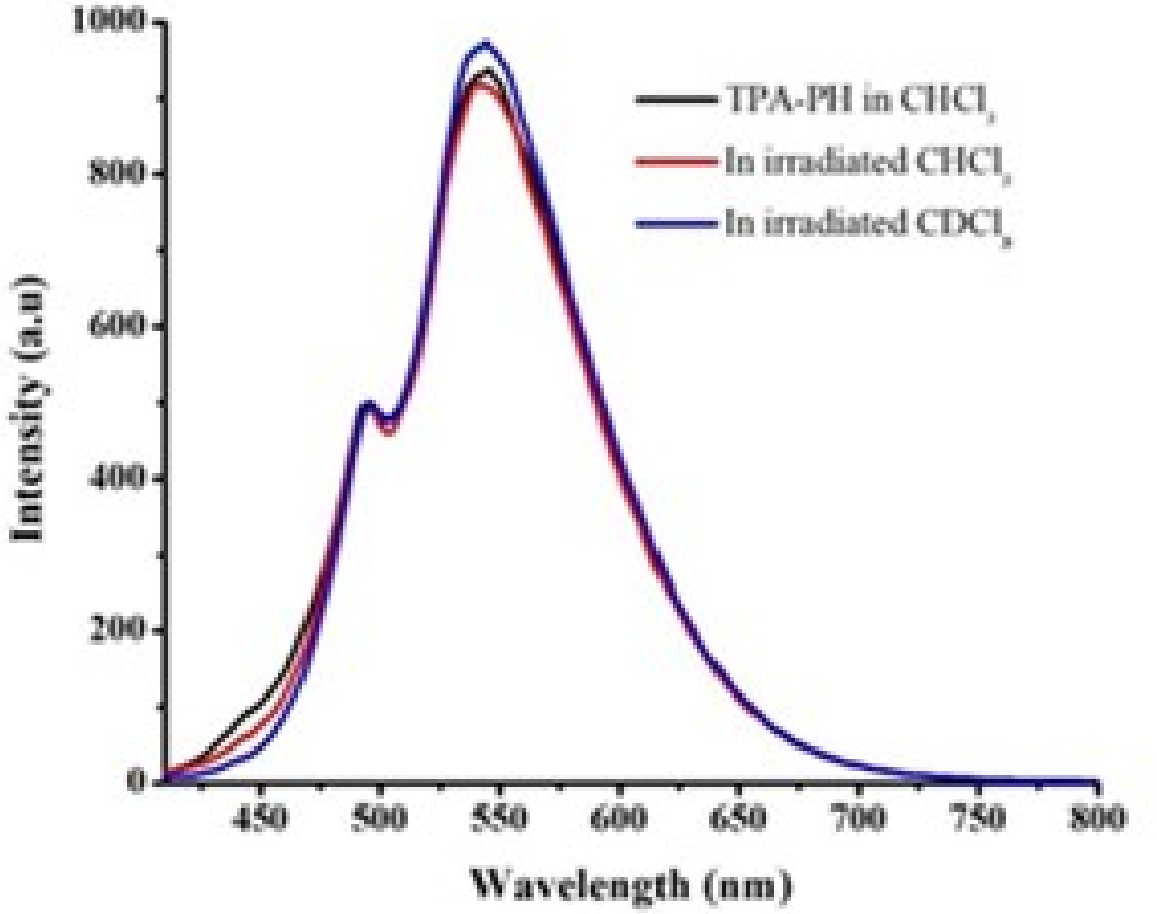

Fig. S51 Fluorescence spectra of TPA-PH in $CHCl_3$ (black), in $CHCl_3$ upon UV irradiation (red) and in $CDCl_3$ upon UV irradiation (blue)

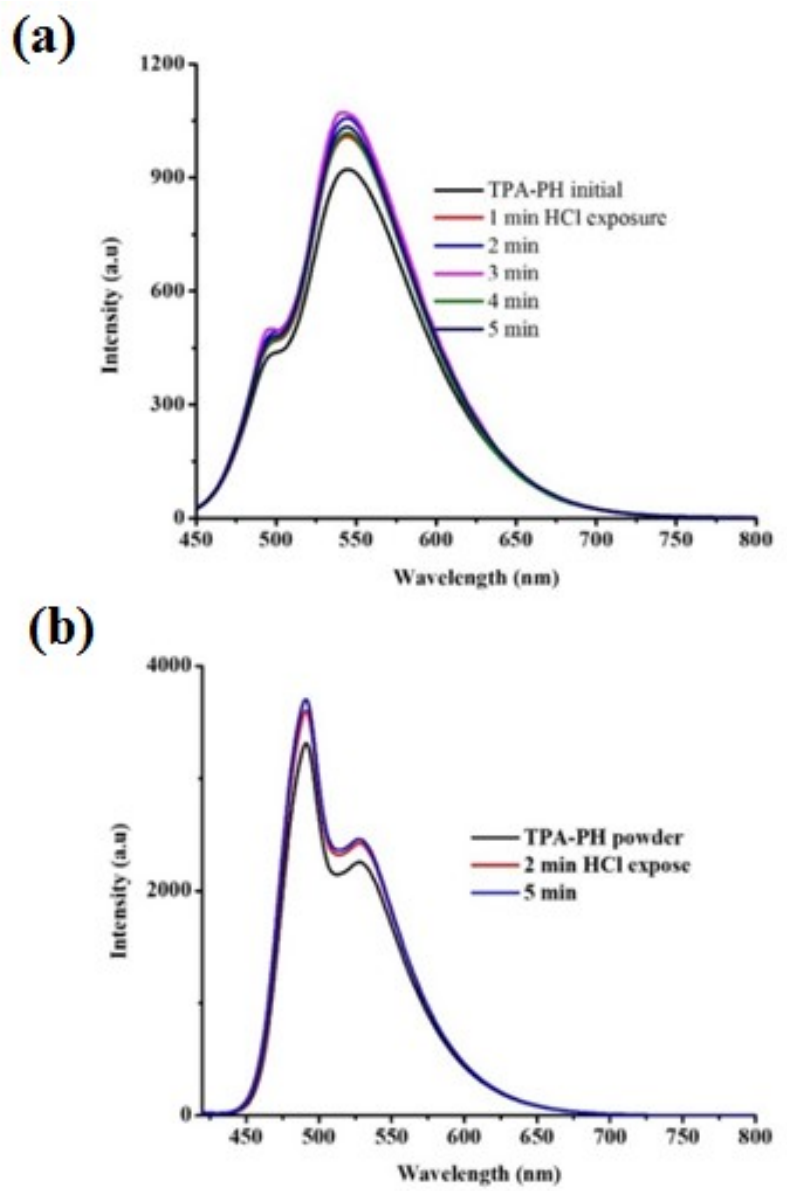

Fig. S52 Fluorescence switching effect of TPA-PH with HCl fuming, in $CHCl_3$ (a) and in solid state (b).